PERGAMON

International Journal of Multiphase Flow 26 (2000) 293–325

International Journal of Multiphase Flow

www.elsevier.com/locate/ijmulflow

On the dispersion of discrete particles moving in a turbulent shear flow

Ph. Pascal, B. Oesterlé*

Laboratoire Universitaire de Mécanique et d'Énergétique de Nancy (LUMEN), ESSTIN, Université Henri Poincaré, Nancy 1, Rue Jean Lamour, F-54500, Vandoeuvre-lès-Nancy, France

Received 5 March 1997; received in revised form 15 March 1999

Abstract

An anisotropic Lagrangian approach is used to investigate the influence of a mean fluid velocity gradient on the motion and on the dispersion of heavy particles suspended in a stationary homogeneous turbulent gas flow. The problem of consistency of the correlation matrices used in first-order stochastic processes is put forward. The accuracy of the method is first checked by comparing the numerical predictions with available experimental results in uniform flow. A second validation test is carried out by comparison with dispersion measurements in a horizontal shear flow. Numerical predictions are then provided in the case of a vertical upward turbulent shear flow, the gravity force field implying a non-zero mean drift velocity between fluid and particles. The transverse particle dispersion is found to be slightly reduced by the presence of a uniform shear. The streamwise particle turbulent intensity is enhanced above the level predicted without shear, whereas, in the direction normal to the flow, the fluctuating velocity of particles are found to be unaffected by the presence of shear. The effect of the lift force due to the mean shear is found to be negligible, except for the mean transverse deviation, which is found however not to be caused only by the lift. The presented numerical results, which confirm and extend the theoretical analysis of others, may explain some experimental observations reported in the literature.

Keywords: Particle dispersion; Lagrangian simulation; Turbulence; Shear flow

* Corresponding author.

0301-9322/00/$ - see front matter
PII: S0301-9322(99)00019-1

1. Introduction

Flows of solid particles or droplets suspended in a turbulent fluid are encountered in many practical situations such as pneumatic conveying, sediment transport, pollution or combustion. In such kinds of flows, the interactions between the particles and the fluid involve two important mechanisms, which are the modification of fluid turbulence by the presence of particles (Hetsroni, 1989; Yarin and Hetsroni; 1994a, b, Crowe et al., 1996), which will not be discussed here, and the particle motion due to fluid turbulent fluctuations. As far as the latter mechanism is concerned, it may be very instructive to investigate the dispersion of particles in a turbulent shear flow, which is a problem of great importance in the near-wall region of confined suspension flows. Several authors, who carried out experiments in boundary layer flows (Rogers and Eaton, 1990) or in pipe flows (Soo et al., 1960; Tsuji and Morikawa, 1982), reported that the streamwise fluctuating velocity of suspended particles may exceed the fluid r.m.s. velocity. A theoretical analysis of such an effect of a mean fluid velocity gradient on the streamwise velocity variance of a small particle suspended in a turbulent flow was proposed by Liljegren (1993). In her study, no body force was considered, and the investigation was restricted to the case of small particles whose drag force obeys the Stokes' law. Liljegren showed that the magnitude of the streamwise r.m.s. velocity of small solid particles suspended in a gas flow is increased by the presence of the mean shear, whereas the transverse particle turbulent intensity is not significantly affected.

The present paper is devoted to the study of the influence of shear on the particle turbulent response and dispersion in a range of finite particle Reynolds numbers, and in the presence of the gravitational body force field. The effect of the shear induced lift force, which may possibly have a significant influence in the near-wall regions, is also studied. Results are obtained by simulating, by means of a Lagrangian technique for anisotropic turbulence, the fluctuating motion and the dispersion of discrete particles in a vertical upward air flow, so that the gravity force acts in the counter-streamwise direction. The turbulence is assumed to be stationary and homogeneous, and the dispersed phase concentration is supposed low enough for the fluid flow not to be altered by the presence of the particles. Before investigating the effect of the mean fluid velocity gradient, some results concerned with the transverse particle dispersion in a turbulent uniform flow, without taking any shear rate into account, are presented and compared with Snyder and Lumley's experiments (Snyder and Lumley, 1971), in order to assess the accuracy of the numerical code. Results concerning the streamwise particle dispersion in the same conditions are also given. Dispersion predictions in a horizontal shear flow are then compared with recently available measurements performed by Huang and Stock (1997), in order to check the capabilities of the proposed simulation method in the presence of shear. Finally, the effect of shear is investigated in a simulated vertical homogeneous shear flow, corresponding to the experimental data of Champagne et al. (1970). Results are given for the streamwise, transverse and cross dispersions, as well as for particle turbulent intensities, and are discussed with relevance to the theoretical analysis of Liljegren (1993).

2. Particle motion in turbulence: governing equations

The three-dimensional fluctuating motion of spherical particles is investigated here by the use of a Lagrangian tracking technique, which lies on the simultaneous computation of a discrete particle trajectory and of the neighbouring fluid particle path, and allows the velocity fluctuations to be predicted by taking into account the space and time correlations. This technique will be described in the next section, after the equations governing the particle motion have been presented. In order to study the motion of a single particle, the fluid and particle instantaneous velocity vectors are split into a mean velocity vector and a fluctuating velocity vector:

$$\mathbf{V}_\mathrm{p} = \overline{\mathbf{V}_\mathrm{p}} + \mathbf{v}_\mathrm{p}, \qquad \mathbf{V}_\mathrm{f} = \overline{\mathbf{V}_\mathrm{f}} + \mathbf{v}_\mathrm{f}, \tag{1}$$

The only non-vanishing component of the mean fluid and particle velocities are along the x_1 (vertical) co-ordinate direction. In case of linear shear, the undisturbed mean fluid velocity depends on the transverse co-ordinate x_2 according to:

$$\overline{V_{\mathrm{f}_1}}(x_2) = \overline{V_{\mathrm{f}_{1_0}}} + \chi x_2, \tag{2}$$

where $\overline{V_{\mathrm{f}_{1_0}}}$ is the value of the mean fluid velocity at $x_2 = 0$ (particle injection point), and χ is the mean shear rate, which is assumed constant. The instantaneous and mean particle Reynolds numbers, Re_p and $\overline{Re_\mathrm{p}}$, based on the instantaneous and mean relative velocity, respectively, are defined by

$$Re_\mathrm{p} = |\mathbf{V}_\mathrm{f} - \mathbf{V}_\mathrm{p}|\frac{d}{\nu} \quad \text{and} \quad \overline{Re_\mathrm{p}} = |\overline{\mathbf{V}_\mathrm{f}} - \overline{\mathbf{V}_\mathrm{p}}|\frac{d}{\nu} \tag{3}$$

where ν is the fluid kinematic viscosity and d denotes the particle diameter. Besides these two particle Reynolds numbers, we introduce a shear Reynolds number, defined as follows:

$$Re_\chi = \frac{|\chi| d^2}{\nu}, \tag{4}$$

The well-known Basset–Boussinesq–Oseen equation, which governs the non-stationary motion of a rigid spherical particle at very small particle Reynolds numbers, was first extended by Tchen (1947), then modified by Corssin and Lumley (1956) and corrected by Maxey and Riley (1983) and Gatignol (1983), who included, in particular, the appropriate Faxen correction for particle motion in a nonuniform flow. The extension proposed by Odar (1966) for higher particle Reynolds numbers has been proved to be incorrect by Mei and Adrian (1992), who derived a modified expression of the kernel of the history force integral, yielding accurate results up to $Re_\mathrm{p} = 100$.

However, in case of a solid particle or a droplet moving in a gas, the particle density is much larger than the fluid density, so that the history force, the added mass force and the displaced mass force can be shown to be negligible as compared to the quasi-stationary drag force. More precisely, the added and displaced mass forces are found to be $O(\frac{u'}{V_\mathrm{r}}\frac{d^2}{\nu T_\mathrm{L}})$ compared to the drag force, where T_L is the Lagrangian integral time scale of the turbulence, u' is an estimate of the fluid r.m.s. velocity, and V_r is the relative velocity of the particle with respect to

the fluid. In the examples considered in the present work, the ratio $\frac{u'}{V_r}\frac{d^2}{\nu T_L}$ ranges from 10^{-2} to 10^{-4}. Nevertheless, such unsteady forces may be of the same order of magnitude than the shear induced lift force for small particle Reynolds numbers, as shown by Maxey and Riley (1983). Since we will be studying the influence of the lift force induced by the mean shear, it is thus necessary to examine the magnitude of the unsteady forces compared to the quasi-stationary transverse force due to the mean fluid velocity gradient.

An expression of the shear lift force on a sphere at small Reynolds number was first theoretically derived by Saffman (1965,1968), whose result has been extended by MacLaughlin (1991). Later, the lift has been numerically predicted by Dandy and Dwyer (1990), and correlated by Mei (1992), for particle Reynolds numbers ranging up to 100. It must be pointed out that such a lift force is related not only to the mean shear, but also to the mean relative velocity between fluid and particle, $\overline{V_{f_1}} - \overline{V_{p_1}}$, which is not zero here because of the external body force field. It is assumed that there is no lift force due to the rotating motion of the particle.

By using the lift expressions of Mei (1992) (see Appendix A), it can be shown that the ratio of the added mass force to the mean lift force is $O(d/T_L\sqrt{\nu\chi})$ in the range of particle Reynolds numbers investigated herein ($0.05 < Re_p < 2.6$; $0 < Re_\chi < 0.01$). Since the ratio $d/(T_L\sqrt{\nu\chi})$ lies in the range 10^{-2} to 10^{-1}, the lift force due to the mean velocity gradient may possibly have a non negligible effect. Furthermore, the added mass force has a zero mean value, contrary to the shear lift force, which has a non-vanishing mean value, related to the mean velocity gradient and to the mean slip velocity. Owing to the assumption of constant shear rate, the mean values of the displaced mass term and of the Faxen term in the history force are also zero. Following the same argument as for the added mass force, such unsteady forces will therefore also be neglected compared to the mean lift force, which will be taken into account in the calculations, in order to examine its influence.

Under such conditions, i.e., only the gravity force, the quasi-stationary drag force and the quasi-stationary shear lift force are considered, the instantaneous equations of motion of a particle, with mass m, in a Cartesian co-ordinate system $Ox_1x_2x_3$, at time t, are:

$$
\begin{aligned}
m\frac{\mathrm{d}V_{p_1}}{\mathrm{d}t} &= \frac{\pi d^2}{4}\frac{1}{2}\rho_f|\mathbf{V}_f - \mathbf{V}_p|\left(V_{f_1} - V_{p_1}\right)C_D - mg_1 \\
m\frac{\mathrm{d}V_{p_2}}{\mathrm{d}t} &= \frac{\pi d^2}{4}\frac{1}{2}\rho_f\left(|\mathbf{V}_f - \mathbf{V}_p|\left(V_{f_2} - V_{p_2}\right)C_D + \left(V_{f_1} - V_{p_1}\right)^2 C_L\right) - mg_2 \\
m\frac{\mathrm{d}V_{p_3}}{\mathrm{d}t} &= \frac{\pi d^2}{4}\frac{1}{2}\rho_f|\mathbf{V}_f - \mathbf{V}_p|\left(V_{f_3} - V_{p_3}\right)C_D - mg_3
\end{aligned}
\tag{5}
$$

where ρ_f is the fluid density, g_i are the gravitational acceleration components, and C_D and C_L denote the drag and lift coefficients, respectively. The best estimation of C_D in a large range of Reynolds numbers is provided by the formula proposed by Morsi and Alexander (1972), which will therefore be used herein for the calculation of the quasi-stationary drag in terms of the instantaneous particle Reynolds number. The lift coefficient C_L will be predicted by the above mentioned correlation of Mei (1992) (the drag and lift coefficient expressions are given in

Appendix A). It must be pointed out that Mei's correlation assumes that the particle and the fluid are moving in the same direction, which is not strictly the case in the present problem. That is why the lift force, which is referred to the streamwise relative velocity $V_{f_1} - V_{p_1}$, is supposed to act only in the x_2-direction, keeping in mind that the only way to express such a shear induced transverse force is an approximate way, due to the lack of available information concerning the exact form of the instantaneous lift.

Eq. (5) can be rewritten as:

$$\frac{dV_{p_i}}{dt} = \frac{d\left(\overline{V_{p_i}} + v_{p_i}\right)}{dt} = \frac{3}{4}\frac{\rho_f}{\rho_p}\left(\frac{\nu}{d^2}C_D Re_p\left(V_{f_i} - V_{p_i}\right) + \frac{\delta_{i2}}{d}C_L\left(V_{f_1} - V_{p_1}\right)^2\right) - g_i \tag{6}$$

where ρ_p denotes the particle material density, and δ_{ij} is the Kronecker symbol.

By solving Eq. (6) for a given fluid instantaneous velocity, the instantaneous particle velocity can be obtained. Calculation has been performed by means of a Lagrangian tracking method, which is described in Section 3.

3. Outlines of the Lagrangian tracking method

In Lagrangian methods, particles are individually tracked through solving the particle equation of motion, and a significant number of particle trajectories are calculated. In order to take into consideration the effect of fluid turbulence on the particle motion, the instantaneous velocity fluctuations of the fluid must be known at each point of the discrete particle trajectory. Lagrangian approaches were first proposed by Peskin and Kau (1976) and Gosman and Ioannides (1981), who introduced the so-called eddy interaction models. Gouesbet et al. (1982,1984) studied the dispersion of particles using Frenkiel functions to approximate the Lagrangian time correlation of the fluid turbulence. In the method of Ormancey and Martinon (1984), the fluid fluctuating velocity at the discrete particle location is generated in taking the fluid velocity longitudinal and transverse correlations into account. The model of Burnage and Moon (1990) lies on the space–time random distributions of the turbulent scales, the mean values of which are the local Lagrangian time scale and Eulerian length scale. Lu et al. (1993) proposed a Lagrangian simulation method in three-dimensional turbulent suspension flows. However, all these models assume that the fluid turbulence is isotropic, as is the case in the comprehensive theoretical analysis on particle dispersion published by Wang and Stock (1993). Recently, Graham (1998) proposed an analytical comparison of Lagrangian particle dispersion models in isotropic turbulence, including the particle-cloud approaches like the stochastic–probabilistic model developed by Chen and Pereira (1997). The first Lagrangian methods for anisotropic turbulence were presented by Berlemont et al. (1990) and Zhou and Leschziner (1991), and an overview of the techniques of modelling turbulent particle dispersion in complex flows was recently given by Shirolkar et al. (1996). The Lagrangian technique used in the present paper follows the principles of the approach proposed by Burry and Bergeles (1993) [hereafter denoted BB], also applied later by Zhou and Leschziner (1996) [ZL], which lies on two consecutive first-order autoregressive processes to predict the fluid instantaneous velocity at the discrete particle location.

In this technique, the discrete particle and the corresponding fluid particle start out from the same position $\mathbf{x}_f(t-\Delta t)=\mathbf{x}_p(t-\Delta t)$ at time level $t-\Delta t$. After one time step Δt, they arrive at $\mathbf{x}_p(t)$ and $\mathbf{x}_f(t)$, respectively. The new discrete particle velocity $\mathbf{V}_p(\mathbf{x}_p(t),t)$ and position $\mathbf{x}_p(t)$ are obtained through numerical integration of the particle equation of motion [6] by means of a Runge–Kutta method. In order that the new discrete particle position $\mathbf{x}_p(t)$ can be used as the starting point of both kinds of particles for the next time step, it is necessary to predict the fluid instantaneous velocity at time t and position $\mathbf{x}_p(t)$. This velocity $\mathbf{V}_f(\mathbf{x}_p(t),t)$ is expressed in terms of the velocity $\mathbf{V}_f(\mathbf{x}_f(t),t)$ in taking into account a given two-point velocity correlation tensor, whereas $\mathbf{V}_f(\mathbf{x}_f(t),t)$ is connected to the known velocity $\mathbf{V}_f(\mathbf{x}_f(t-\Delta t),t-\Delta t)$ throughout the Lagrangian time correlation tensor. The corresponding procedure will be described in Sections 3.1 and 3.2.

Although our model is not basically different from the models presented by BB or ZL, it must be mentioned, however, that these authors used Frenkiel correlations, which are not consistent with the principles of generating the fluid instantaneous velocity by means of first-order time series model: it will be theoretically proved, in Section 3.3, that only exponential correlation matrices can be used in such autoregressive processes. A way of building exponential correlation matrices in a shear flow is proposed in Section 3.4. Contrary to BB and ZL, the original technique developed by Berlemont et al. (1990) is theoretically correct in what concerns the fluid particle tracking, but it is based on very large correlation matrices, and practical application is restricted to two-dimensional flows. Moreover, the prediction of the fluid instantaneous velocity at the solid particle location, $\mathbf{V}_f(\mathbf{x}_p(t),t)$, suffers from the same drawbacks as in BB or ZL, and the proposed spatial cross-correlations do not amount to the correct Reynolds stresses when the distance is zero.

3.1. Prediction of the instantaneous fluid velocity $V_f(x_f(t),t)$

Following ZL or BB, the time correlation is introduced to the method in expressing the fluid fluctuating velocity at time t and position $\mathbf{x}_f(t)$, denoted by $\mathbf{v}_f(\mathbf{x}_f(t),t)$, as

$$\mathbf{v}_f(\mathbf{x}_f(t),t)=\mathbf{H}(t,\Delta t)\mathbf{v}_f\big(\mathbf{x}_f(t-\Delta t),t-\Delta t\big)+\mathbf{d}(t,\Delta t) \tag{7}$$

where $\mathbf{H}$ is a matrix which takes into consideration all the effects from previous time steps, and $\mathbf{d}$ is a random vector obeying a Gaussian conditional PDF, which takes into account the randomness due to turbulence as well as the flow anisotropy. Multiplying Eq. (7) by the transpose $\mathbf{v}_f^T(\mathbf{x}_f(t-\Delta t),t-\Delta t)$ and taking the expectations of each side in order to get the autocovariance matrix of $\mathbf{v}_f$, we can express the matrix $\mathbf{H}$ in terms of the Lagrangian correlation coefficients $R_{ij}(t,\Delta t)$, defined by (no summation on i or j):

$$\overline{v_{f_i}(\mathbf{x}_f(t),t)v_{f_j}\big(\mathbf{x}_f(t-\Delta t),t-\Delta t\big)}=R_{ij}(t,\Delta t)u'_{i_t}u'_{j_{t-\Delta t}} \tag{8}$$

where u'_{i_t} denotes the r.m.s. velocity $\sqrt{\overline{v_{f_i}^2(\mathbf{x}_f(t),t)}}$. Note that u'_{i_t} and $R_{ij}(t,\Delta t)$ depend on t in case of non-homogeneous turbulence, even if stationary turbulence is assumed. Denoting by $\{a_{ij}\}$ a matrix whose elements are the quantities a_{ij}, we obtain:

$$\mathbf{H}(t,\Delta t) = \left\{ R_{ij}(t,\Delta t) u'_{i_t} u'_{j_{t-\Delta t}} \right\} \left\{ R_{ij}(t,0) u'_{i_{t-\Delta t}} u'_{j_{t-\Delta t}} \right\}^{-1} \tag{9}$$

Similarly, the covariance matrix of vector **d** can be shown to obey (see ZL for analytical details):

$$\mathbf{d}(t,\Delta t)\mathbf{d}^{\mathrm{T}}(t,\Delta t) = \left\{ \overline{d_i d_j} \right\}_{(t,\Delta t)} = \left\{ R_{ij}(t,0) u'_{i_t} u'_{j_t} \right\} - \mathbf{H}(t,\Delta t) \left\{ R_{ij}(t,\Delta t) u'_{i_{t-\Delta t}} u'_{j_t} \right\} \tag{10}$$

which makes it possible to generate the components of **d** using the Cholesky algorithm as previously done by Berlemont et al. (1990) and ZL. To summarise, the process described by Eq. (7) can be used to generate the turbulent velocity fluctuations along the path of any fluid particle, provided that the Lagrangian time correlation tensor is known for any Δt (therefore including the knowledge of $R_{ij}(t,0)$, which is the Reynolds stress tensor at point $\mathbf{x}_{\mathrm{f}}(t)$). Further requirements concerning the time correlation tensor will be addressed in Section 3.3.

3.2. Prediction of the instantaneous fluid velocity at point $x_{\mathrm{p}}(t)$

Following the suggestion by BB, a similar concept is used for the prediction of the fluid fluctuating velocity at the discrete particle location, according to:

$$\mathbf{v}_{\mathrm{f}}\big(\mathbf{x}_{\mathrm{p}}(t),t\big) = \mathbf{K}\big(\mathbf{x}_{\mathrm{p}}(t),\xi\big)\mathbf{v}_{\mathrm{f}}(\mathbf{x}_{\mathrm{f}}(t),t) + \mathbf{e}\big(\mathbf{x}_{\mathrm{p}}(t),\xi\big) \tag{11}$$

where $\xi = \mathbf{x}_{\mathrm{p}} - \mathbf{x}_{\mathrm{f}}$, the separation vector between the two positions, is taken into account in expressing the matrix **K** in terms of the spatial correlations, and **e** is a vector representing the randomness due to turbulence. In order that the spatial correlations may be expressed in terms of the scalar quantity $\Delta r = |\xi|$, it is convenient to write Eq. (11) in a local co-ordinate system defined in such a manner that v_{f_1} is collinear to the vector $\mathbf{x}_{\mathrm{p}} - \mathbf{x}_{\mathrm{f}}$ (v_{f_α} being the α-component of the fluid fluctuating velocity in such a reference frame). Handling Eq. (11) in the same manner as Eq. (7) above leads to the following expression of the matrix **K**:

$$\mathbf{K}\big(\mathbf{x}_{\mathrm{p}},\Delta r\big) = \left\{ Q_{\alpha\beta}\big(\mathbf{x}_{\mathrm{p}},\Delta r\big) u'_{\alpha_{\mathrm{p}}} u'_{\beta_{\mathrm{f}}} \right\} \left\{ Q_{\alpha\beta}\big(\mathbf{x}_{\mathrm{p}},0\big) u'_{\alpha_{\mathrm{f}}} u'_{\beta_{\mathrm{f}}} \right\}^{-1} \tag{12}$$

where $u'_{\alpha_{\mathrm{p}}} = \sqrt{\overline{v^2_{\mathrm{f}_\alpha}(\mathbf{x}_{\mathrm{p}}(t),t)}}$ and $u'_{\alpha_{\mathrm{f}}} = \sqrt{\overline{v^2_{\mathrm{f}_\alpha}(\mathbf{x}_{\mathrm{f}}(t),t)}}$, the components $Q_{\alpha\beta}$ of the two-point velocity correlation tensor being defined by

$$\overline{v_{\mathrm{f}_\alpha}\big(\mathbf{x}_{\mathrm{p}}(t),t\big) v_{\mathrm{f}_\beta}(\mathbf{x}_{\mathrm{f}}(t),t)} = Q_{\alpha\beta}\big(\mathbf{x}_{\mathrm{p}},\Delta r\big) u'_{\alpha_{\mathrm{p}}} u'_{\beta_{\mathrm{f}}} \tag{13}$$

As for the vector **d** in Section 3.1, the vector **e** can be generated by means of the Cholesky algorithm after its covariance matrix has been calculated by

$$\left\{ \overline{e_\alpha e_\beta} \right\}_{(\mathbf{x}_{\mathrm{p}},\Delta r)} = \left\{ Q_{\alpha\beta}\big(\mathbf{x}_{\mathrm{p}},0\big) u'_{\alpha_{\mathrm{p}}} u'_{\beta_{\mathrm{p}}} \right\} - \mathbf{K}\big(\mathbf{x}_{\mathrm{p}},\Delta r\big) \left\{ Q_{\alpha\beta}\big(\mathbf{x}_{\mathrm{p}},\Delta r\big) u'_{\alpha_{\mathrm{f}}} u'_{\beta_{\mathrm{p}}} \right\} \tag{14}$$

Here again, the main difficulty lies in the appropriate assessment of the correlation tensor in order to enable a new fluid fluctuating velocity to be properly generated at location $\mathbf{x}_{\mathrm{p}}$, so that the whole process can be repeated using $\mathbf{x}_{\mathrm{p}}$ as the starting point for the new time step. Although the tensor $Q_{\alpha\beta}$ may generally be different from the fluid Eulerian spatial correlation

tensor, it has been recently shown by Ushijima and Perkins (1998) that the two-point correlation tensor defined by Eq. (13) can be approached by the fluid Eulerian spatial correlation tensor when the effect of gravity is present. In the following subsection, we describe the conditions that have to be fulfilled by the correlation matrices for the particle tracking process to be consistent.

3.3. Consistency requirements for the correlation tensors

As a matter of fact, first-order autoregressive processes involved in Eqs. (7) and (11) are discrete approximations of continuous processes represented by a first-order stochastic differential equation (see Harvey, 1989). In case of homogeneous isotropic turbulence, where the three components of the velocity can be treated independently, the differential equation associated with Eq. (7) takes the form of the well-known Langevin equation. Therefore, using Eq. (7) in such an one-dimensional case comes down to assume that the velocity of a fluid particle obeys the Langevin equation, which is known to lead to an exponentially decaying autocorrelation function (Sawford, 1991; Shirolkar et al., 1996). More generally, for any vectorial autoregressive process obeying the form of Eqs. (7) or (11), the matrix $\mathbf{H}$ (or $\mathbf{K}$) must meet some requirements in order that the coherent nature of the turbulent eddies be correctly taken into account. Let us examine the consequences of describing the time evolution of the fluctuating velocity vector by Eq. (7), under the assumption of stationary Lagrangian statistics (which is the case herein since we are concerned with steady homogeneous turbulence). Multiplying each side of this equation by $\mathbf{v}_{\mathrm{f}}^{\mathrm{T}}(\mathbf{x}_{\mathrm{f}}(t-\tau),t-\tau)$, and denoting by $\Gamma(\tau)$ the Lagrangian autocovariance matrix obtained through averaging (i.e. $\Gamma(\tau)=\{\overline{v_{fi}(t)v_{fj}(t-\tau)}\}$), we get:

$$\Gamma(\tau)=\mathbf{H}(\Delta t)\Gamma(\tau-\Delta t)\quad\forall\Delta t,\ \tau>0 \tag{15}$$

and, similarly:

$$\Gamma(\tau-\Delta t)=\mathbf{H}(\Delta t')\Gamma(\tau-\Delta t-\Delta t')\quad\forall\Delta t,\Delta t',\ \tau>\Delta t \tag{16}$$

so that we must have:

$$\Gamma(\tau)=\mathbf{H}(\Delta t)\mathbf{H}(\Delta t')\Gamma(\tau-\Delta t-\Delta t')\quad\forall\Delta t,\ \Delta t' \tag{17}$$

and, according to Eq. (15) in replacing Δt by $\Delta t+\Delta t'$:

$$\Gamma(\tau)=\mathbf{H}(\Delta t+\Delta t')\Gamma(\tau-\Delta t-\Delta t')\quad\forall\Delta t,\ \Delta t' \tag{18}$$

It is therefore required, for consistency of the stochastic process, that the matrix $\mathbf{H}$ satisfies:

$$\mathbf{H}(\Delta t)\mathbf{H}(\Delta t')=\mathbf{H}(\Delta t+\Delta t')\quad\forall\Delta t,\ \Delta t' \tag{19}$$

a condition which can only be fulfilled by the exponential matrical form $\mathbf{H}(\Delta t)=\mathrm{e}^{-\mathbf{A}\Delta t}$, where $\mathbf{A}$ is a positive-definite matrix in order that the components of $\mathbf{H}$ tend to zero for $\tau\rightarrow\infty$ (it may be noticed that, for constant Δt, the same result can be obtained in a more straightforward manner by putting $\tau=n\Delta t$ in Eq. (15) and substituting repeatedly for lagged

values of $\Gamma(\tau)$, leading to $\mathbf{H}(n\Delta t) = [\mathbf{H}(\Delta t)]^n$, thus showing the necessary exponential form of the matrix $\mathbf{H}$). Hence, according to Eq. (15) written for $\Delta t = \tau$, the only consistent form of the autocovariance matrix is:

$$\Gamma(\tau) = \mathrm{e}^{-\mathbf{A}\tau}\Gamma(0) \tag{20}$$

where $\Gamma(0)$ is the Reynolds stress tensor.

This means that, whatever the autocovariance matrix is used to calculate the matrix $\mathbf{H}$ according to Eq. (9), the first order time series will unavoidably generate an exponential autocovariance matrix. Such a result, which is in accordance with the above-mentioned exponentially decaying autocorrelation function in case of homogeneous isotropic turbulence, is very important because using any other form of correlation functions in such first-order autoregressive processes (as was done, for example, by ZL or BB who used Frenkiel functions) may lead to spurious results after a large number of time steps. In order to illustrate the result of using arbitrary given correlation functions, let us consider the one-dimensional case of stationary homogeneous isotropic turbulence, where the method of generating $v_\mathrm{f}(t)$ according to Eq. (7) would take the simple scalar form:

$$v_\mathrm{f}(t) = H(\Delta t)v_\mathrm{f}(t-\Delta t) + d(t) \tag{21}$$

Here the matrix $\mathbf{H}$ is replaced by the scalar H, whose expression in terms of the initially given correlation function $R(\Delta t)$ is merely $H(\Delta t) = R(\Delta t)$, according to Eq. (9). Using a time step Δt_0, multiplying each side of Eq. (21) by $v_\mathrm{f}(t - n\Delta t_0)$ and averaging leads to the autocovariance $\Gamma(n\Delta t_0)$:

$$\Gamma(n\Delta t_0) = \overline{v_\mathrm{f}(t)v_\mathrm{f}(t-n\Delta t_0)} = R(\Delta t_0)\overline{v_\mathrm{f}(t-\Delta t_0)v_\mathrm{f}(t-n\Delta t_0)} = R(\Delta t_0)\Gamma\big((n-1)\Delta t_0\big) \tag{22}$$

This relationship can be written for any $n \geq 1$, so that:

$$\Gamma(n\Delta t_0) = R(\Delta t_0)\Gamma\big((n-1)\Delta t_0\big) = (R(\Delta t_0))^2\Gamma\big((n-2)\Delta t_0\big) = \cdots = (R(\Delta t_0))^n\Gamma(0) \tag{23}$$

In terms of the time lag $\tau = n\Delta t_0$, we can therefore write:

$$\overline{v_\mathrm{f}(t)v_\mathrm{f}(t-\tau)} = \Gamma(\tau) = \overline{v_\mathrm{f}^2}(R(\Delta t_0))^{\tau/\Delta t_0} = \overline{v_\mathrm{f}^2}\exp\left(\frac{\tau}{\Delta t_0}\ln R(\Delta t_0)\right) \tag{24}$$

thus showing that the autocorrelation generated by the stochastic process is an exponential function whatever the form of the initially given function $R(\Delta t)$. Except if $R(\Delta t) = \mathrm{e}^{-\Delta t/T}$, the resulting autocorrelation will depend on the time step Δt_0. Using, for example, the Frenkiel function $R(\Delta t) = \exp(-\Delta t/2T)\cos(\Delta t/2T)$ (whose integral time scale is T) for the generation of fluctuating velocities according to Eq. (21) will yield an exponential autocorrelation obeying

$$\frac{\overline{v_\mathrm{f}(t)v_\mathrm{f}(t-\tau)}}{\overline{v_\mathrm{f}^2}} = \exp\left\{-\frac{\tau}{\Delta t_0}\left(\frac{\Delta t_0}{2T} - \ln\left(\cos\frac{\Delta t_0}{2T}\right)\right)\right\} \tag{25}$$

or, for small Δt_0:

$$\frac{\overline{v_{\mathrm{f}}(t)v_{\mathrm{f}}(t-\tau)}}{\overline{v_{\mathrm{f}}^2}} \approx \exp\left\{ -\frac{\tau}{2T}\left(1+\frac{\Delta t_0}{4T}\right)\right\} \tag{26}$$

which shows that the effective integral time scale of the generated velocity fluctuations will be $T^* \approx \frac{2T}{1+\Delta t_0/4T} \approx 2T$ instead of the desired value which is T!

Of course, any form of explicitly given correlation functions, like Frenkiel-type functions (with one or several negative loops) or the form suggested by Sawford (1991), without negative loop (but exhibiting the correct parabolic behaviour at the origin), can be generated by means of stochastic processes, but such processes are not first-order ones, which means that the velocity at time t depends on more lagged values. Consequently, it is not possible to use them in the typical BB approach, because it would be necessary to know (for a second-order process, for example) the velocity of the same fluid particle at $t-2\Delta t$ and $t-\Delta t$ (or, equivalently, the velocity and the acceleration at time $t-\Delta t$) to calculate its velocity at time t, which is not the case for the reason that the spatial transfer makes the tracked fluid particle to change at each time step.

In a similar manner, the process used in Eq. (11) to express the velocity $\mathbf{v}_{\mathrm{f}}(\mathbf{x}_{\mathrm{p}}(t))$ as a function of $\mathbf{v}_{\mathrm{f}}(\mathbf{x}_{\mathrm{f}}(t))$ can be shown to be consistent with an exponential matrix for the two-point velocity covariance tensor. The way such correlation matrices are built is explained in Section 3.4.

3.4. Correlation matrices used herein for homogeneous shear flow

As we are interested in predicting particle dispersion in homogeneous or quasi-homogeneous shear flows, we consider the following Reynolds stress tensor:

$$\Gamma(0) = \begin{Bmatrix} \overline{v_{\mathrm{f}_1}^2} & C_{12}\sqrt{\overline{v_{\mathrm{f}_1}^2}}\sqrt{\overline{v_{\mathrm{f}_2}^2}} & 0 \\ C_{12}\sqrt{\overline{v_{\mathrm{f}_1}^2}}\sqrt{\overline{v_{\mathrm{f}_2}^2}} & \overline{v_{\mathrm{f}_2}^2} & 0 \\ 0 & 0 & \overline{v_{\mathrm{f}_3}^2} \end{Bmatrix} \tag{27}$$

where C_{12} is the constant one-point correlation coefficient defined by $\overline{v_{\mathrm{f}_1}v_{\mathrm{f}_2}} = C_{12}\sqrt{\overline{v_{\mathrm{f}_1}^2}}\sqrt{\overline{v_{\mathrm{f}_2}^2}}$, whose value lies between -0.4 and -0.5 according to available experimental data in such homogeneous shear flows. In order to build the matrix $\mathbf{H}(\tau)$, it is necessary to prescribe some form of the matrix $\mathbf{A}$. From the particular form of the Reynolds stress tensor given by (27), it may be suggested, among various other solutions, trying to find the exponential matrix $\mathbf{H}(\tau)$ by using a matrix $\mathbf{A}$ exhibiting the same simple pattern. We are therefore led to the following expression, which gives the most general form of such a matrix in terms of its eigenvalues $\tau_1^{-1},\tau_2^{-1},\tau_3^{-1}$ (which will be shown later to be connected to the Lagrangian integral time scales), where a, b are adjustable parameters:

$$\mathbf{A} = \begin{Bmatrix} a\tau_1^{-1} + (1-a)\tau_2^{-1} & b\left(\tau_1^{-1} - \tau_2^{-1}\right) & 0 \\ \dfrac{a(1-a)}{b}\left(\tau_1^{-1} - \tau_2^{-1}\right) & (1-a)\tau_1^{-1} + a\tau_2^{-1} & 0 \\ 0 & 0 & \tau_3^{-1} \end{Bmatrix} \tag{28}$$

The exponential matrix $\mathbf{H} = e^{-\mathbf{A}\tau}$ can then be built by $\mathbf{H} = \mathbf{L}e^{-\mathbf{A}^*\tau}\mathbf{L}^{-1}$, where $\mathbf{A}^* = \mathbf{L}^{-1}\mathbf{A}\mathbf{L}$ is the diagonal form of the matrix $\mathbf{A}$, so that $\mathrm{e}^{-\mathbf{A}^*\tau}$ is the diagonal matrix whose elements are $\mathrm{e}^{-\tau/\tau_i}$. By means of Eqs. (20) and (27), and using the definition of the correlation coefficients as given by Eq. (8), the non-zero components of the corresponding correlation tensor can be shown to be:

$$\begin{aligned} R_{11}(\tau) &= (a + bmC_{12})\mathrm{e}^{-\tau/\tau_1} + (1 - a - bmC_{12})\mathrm{e}^{-\tau/\tau_2} \\ R_{21}(\tau) &= \frac{1-a}{bm}(a + bmC_{12})\mathrm{e}^{-\tau/\tau_1} - \frac{a}{bm}(1 - a - bmC_{12})\mathrm{e}^{-\tau/\tau_2} \\ R_{12}(\tau) &= (bm + aC_{12})\mathrm{e}^{-\tau/\tau_1} - \left(bm - (1-a)C_{12}\right)\mathrm{e}^{-\tau/\tau_2} \\ R_{22}(\tau) &= \frac{1-a}{bm}(bm + aC_{12})\mathrm{e}^{-\tau/\tau_1} + \frac{a}{bm}\left(bm - (1-a)C_{12}\right)\mathrm{e}^{-\tau/\tau_2} \\ R_{33}(\tau) &= \mathrm{e}^{-\tau/\tau_3} \end{aligned} \tag{29}$$

where $m = \sqrt{\overline{v_{\mathrm{f}_2}^2}}/\sqrt{\overline{v_{\mathrm{f}_1}^2}}$. From symmetry requirements, i.e. $R_{12} = R_{21}$, we must have:

$$bm(bm + aC_{12}) = (1-a)(a + bmC_{12}) \tag{30}$$

so that there is finally only one free parameter in the formulation of the fluid Lagrangian correlation tensor according to Eq. (29). Acceptable values of a lie in the range which leads to real values of bm from Eq. (30), namely $-\varepsilon \le a \le 1 + \varepsilon$, where $\varepsilon = \frac{1}{2}(1 - \frac{1}{\sqrt{1-C_{12}^2}})$. As can be

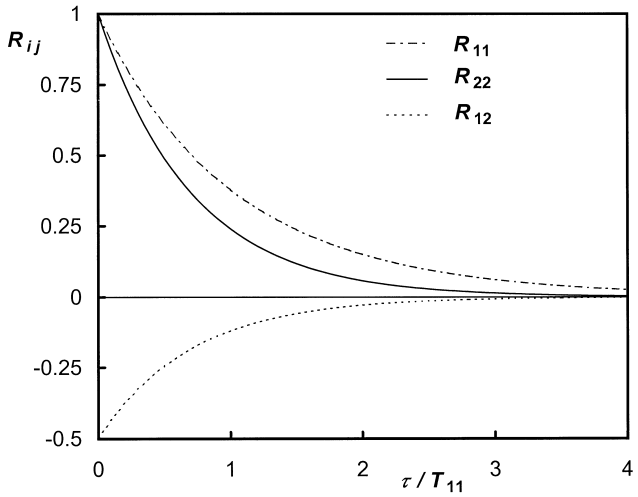

Fig. 1. Examples of Lagrangian correlations meeting the consistency requirements of first-order stochastic processes.

seen from Eqs. (29) and (30), putting $a = 0.5$ leads to $R_{11} = R_{22}$, whereas putting $a = 0$ leads to the same result as $a = 1$ except that τ_1 and τ_2 are inversed. In the hereafter presented calculations, the simplest case $a = 1$ was considered, since this value leads to the simplest form of the matrices $\mathbf{A}$,$\{R_{ij}\}$ and $\mathbf{H}$, and to physically reasonable shapes of the correlations (see Fig. 1). In this case, the correlation tensor takes the simple form:

$$\{R_{ij}(\tau)\} = \begin{Bmatrix} (1 - C_{12}^2)e^{-\tau/\tau_1} + C_{12}^2 e^{-\tau/\tau_2} & C_{12}e^{-\tau/\tau_2} & 0 \\ C_{12}e^{-\tau/\tau_2} & e^{-\tau/\tau_2} & 0 \\ 0 & 0 & e^{-\tau/\tau_3} \end{Bmatrix} \tag{31}$$

Integration of the proposed expressions of $R_{ij}(\tau)$ leads to the relationships between τ_1,τ_2, and the Lagrangian integral time scales T_{11}, T_{22} (τ_3 being obviously equal to T_{33}):

$$\tau_1 = \frac{1}{1 - C_{12}^2}(T_{11} - C_{12}^2 T_{22})$$

$$\tau_2 = T_{22} \tag{32}$$

which can be verified to yield $\int_0^\infty R_{ii}(\tau)\,\mathrm{d}\tau = T_{ii}$. The autocorrelation matrix form suggested in Eq. (31) corresponds to the following matrix $\mathbf{H}$:

$$\mathbf{H}(\Delta t) = \begin{Bmatrix} e^{-\Delta t/\tau_1} & \frac{C_{12}}{m}(e^{-\Delta t/\tau_1} - e^{-\Delta t/\tau_2}) & 0 \\ 0 & e^{-\Delta t/\tau_2} & 0 \\ 0 & 0 & e^{-\Delta t/\tau_3} \end{Bmatrix} \tag{33}$$

which can be verified to actually be an exponential matrix, i.e., to satisfy the condition of Eq. (19).

An example of the shape of the Lagrangian correlations R_{11},R_{22},R_{12} as a function of the dimensionless time τ/T_{11} is illustrated by Fig. 1 in the case $C_{12} = -0.5$,$T_{22}/T_{11} = 0.7$. Although the proposed formulation does not allow the correlation functions to include negative loops, it is believed that such a minor drawback should be preferred rather than using correlations which are not consistent with the time series adopted to generate the fluid velocity fluctuations. The problem of the behaviour of the proposed correlations at small τ (non-vanishing slope at the origin) will be examined in testing the time step influence on the dispersion results presented in the next section.

The same approach is used in order to obtain consistent and physically reasonable expressions of the two-point velocity correlations which are needed for the spatial transfer from point $\mathbf{x}_\mathrm{p}(t)$ to point $\mathbf{x}_\mathrm{f}(t)$, according to Eq. (11). The resulting form of matrix $\mathbf{K}$ is therefore:

$$\mathbf{K}(\Delta r) = \begin{Bmatrix} e^{-\Delta r/\lambda_1} & \frac{C_{12}}{m}(e^{-\Delta r/\lambda_1} - e^{-\Delta r/\lambda_2}) & 0 \\ 0 & e^{-\Delta r/\lambda_2} & 0 \\ 0 & 0 & e^{-\Delta r/\lambda_3} \end{Bmatrix} \tag{34}$$

where λ_2,λ_2, are connected to the fluid integral length scales L_{ii} by relationships similar to Eq. (32), and $\lambda_3 = L_{33}$.

The way the fluid integral scales T_{ii} and L_{ii} are evaluated will be described in the next section, where validation tests are carried out in two kinds of turbulent flows, namely a uniform flow and a horizontal linear shear flow.

4. Code validation in uniform and shear flow

Before studying the particle dispersion in a vertical shear flow, the capability of the present numerical Lagrangian simulation is first tested, in Section 4.1, through comparison with the experiments of Snyder and Lumley (1971) [hereafter denoted SL], performed in a nearly homogeneous isotropic turbulence. In Section 4.2, a second validation test is proposed against the recent experimental results of Huang and Stock (1997) [HS] in a horizontal linear shear flow.

4.1. Simulation of the experiments of Snyder and Lumley (1971)

SL measured the transverse particle dispersion in the grid-generated turbulence of a vertical wind tunnel. The particle densities and diameters, as well as terminal relative velocities and relaxation times, are given in Table 1.

Particles were injected at $x_1/M = 20$, where x_1 is the distance from the grid, and $M = 2.54$ cm is the grid spacing. Single particle trajectories were photographically tracked from $x_1/M = 68$–168. The mean velocity of the upward turbulent air flow, $\overline{V_{f_1}}$, was set at 6.55 m/s, and the transverse mean velocities were zero. The turbulent air flow was nearly isotropic (therefore $C_{12} = 0$), and obeyed the following experimental decay laws:

$$\frac{\overline{V_{f_1}}^2}{\overline{v_{f_1}}^2} = 42.4\left(\frac{x_1}{M} - 16\right) \tag{35}$$

and

Table 1
Particles used in Snyder and Lumley's experiments (Snyder and Lumley, 1971)

	Hollow glass	Corn pollen	Glass	Copper
Diameter d (μm)	46.5	87.0	87.0	46.5
Density ρ_p (kg/m^3)	260	1000	2500	8900
Terminal relative velocity V_t (m/s)	0.0167	0.198	0.442	0.483
Relaxation time τ_p (s) at relative velocity V_t	0.0017	0.0202	0.0451	0.0492
Reynolds number at relative velocity V_t	0.052	1.15	2.56	1.50

$$\frac{\overline{V_{f_1}}^2}{\overline{v_{f_2}}^2} = \frac{\overline{V_{f_1}}^2}{\overline{v_{f_3}}^2} = 39.4\left(\frac{x_1}{M} - 12\right) \tag{36}$$

For the purpose of numerical simulation, the fluid Lagrangian time scale $T_L(= T_{ii}\ \forall i)$ is supposed to obey, at any point downstream of the grid, the following general relationship, where u'^2 is defined by $u'^2 = \frac{1}{3}(\overline{v_{f_1}^2} + \overline{v_{f_2}^2} + \overline{v_{f_3}^2})$, and where ε is the turbulent kinetic energy dissipation rate:

$$T_L = C_T \frac{u'^2}{\varepsilon} \tag{37}$$

In case of the present nearly isotropic flow, the constant C_T is taken equal to 0.235 (according to Hinze, 1975, pp. 397, 426: $C_T = 2/C$ with $C = 8.5$), as was done, among others, by Lu et al. (1993) or Huilier et al. (1996). The dissipation rate ε can be obtained from turbulent kinetic energy conservation equation, which leads to:

$$\varepsilon = -\frac{dk}{dt} = -\overline{V_{f_1}}\frac{dk}{dx_1} = \frac{\overline{V_{f_1}}^3}{2M}\left(\frac{1}{42.4}\left(\frac{x_1}{M} - 16\right)^{-2} + \frac{1}{39.4}\left(\frac{x_1}{M} - 12\right)^{-2}\right) \tag{38}$$

where $k = (3/2)u'^2$ is the turbulent kinetic energy.

As already mentioned, the length scales L_{ii} to be used for the spatial transfer according to Eq. (11) may be assumed to be equal to the Eulerian length scales, and therefore to obey the following general relationship, which was used by many workers (see Berlemont et al., 1990, Zhou and Leschziner, 1991, Shirolkar et al., 1996) due to lack of any more satisfactory expression:

$$L_{ii} = C_{Li} T_{ii} \sqrt{\overline{v_{f_i}^2}} \tag{39}$$

where T_{ii} is to be replaced here by T_L as given by (37). In order to apply such expressions of the length scales in case of SL's experiments, we have to take into account that the ratio between longitudinal and lateral Eulerian length scales was found by these authors to be about 2.5 (instead of the theoretical value of 2 in perfectly isotropic turbulence), and that the longitudinal length scale was assessed at about 3 to 4 cm. From such requirements, the following values of coefficients C_{Li} are chosen here: $C_{L1} = 5$; $C_{L2} = C_{L3} = 2$. This choice leads to a longitudinal length scale which is close to the experimental value, contrary to some other workers who simulated SL's experiments by using $C_{L1} = 2.5$, thus largely underestimating the length scales (Lu et al., 1993, Shirolkar and McQuay, 1998).

The particle dispersion can be quantified by computing, at each time step, the mean square displacements of the particles by:

$$\langle x_i^2 \rangle = \langle \left(x_{p_i} - \langle x_{p_i} \rangle\right)^2 \rangle = \langle x_{p_i}^2 \rangle - \langle x_{p_i} \rangle^2, \tag{40}$$

where $\langle \cdot \rangle$ denotes ensemble average. Numerical simulations have been carried out with a time step $\Delta t = 0.2$ ms for the hollow glass particles, and $\Delta t = 1$ ms for the heavier particles. Such values are much lower than both the particle relaxation time and the dissipation time scale of

the turbulence (10 to 30 ms). Averaging has been performed over 20,000 particle trajectories, a sufficiently large number for a fair statistical convergence to be obtained, as shown by Table 2, where transverse dispersion predictions using 10,000, 20,000 and 40,000 particles are compared.

Comparisons between SL's results and the numerical predictions are illustrated by Fig. 2, which is a plot of the mean square displacement in the x_2-direction, as a function of the time t elapsed from the first camera station, located at $x_1/M = 68$. In this figure, numerical results are represented by lines, while symbols are for the experimental data. Agreement between computed and experimental particle transverse dispersions can be seen to be satisfactory, although significant differences are observed for heavy particles, whose long-time dispersion is somewhat overestimated, as well as for pollen particles, whose dispersion is underpredicted. In case of glass and copper particles, such discrepancies, which have also been observed by other workers, like Chen and Crowe (1984), Lu et al. (1993), or Huilier et al. (1996), might be due to the approximations used in the spatial correlations, whose influence is more crucial for heavy particles owing to their significant drift velocity. Concerning the pollen particles, the discrepancy (also observed by Shirolkar and McQuay, 1998) may possibly be explained by an underestimation of the drag force, which is computed using the assumption that particles are perfectly spherical.

The discrimination levels used by SL in their experiments (the maximum displacement between two adjacent cameras was 16.5 mm for the hollow glass beads and 15.2 mm for the other particles) as well as the limits of the field size (which was 20.32 cm wide) were taken into account in the results presented in Fig. 2. However, the influence of such limitations was found to be negligible except for the hollow glass beads, whose predicted dispersion is reduced (by about 5%) compared to the dispersion obtained without any rejection, the rejection rate being about 1.8%.

Due to the adopted approach and to the corresponding consistency requirements mentioned in the previous section, the correlations used herein are known to exhibit a non-physical behaviour at small time lags, i.e., the parabolic portion near the origin is not represented. That is the reason why the influence of the time step had to be examined, particularly for the hollow glass particles, whose small relaxation time requires a small time step. Results illustrated by Table 3 show that the time step influence is not significant, which is presumably a positive consequence of ensuring consistency between the stochastic process and the prescribed

Table 2
Effect of the number of simulated particle trajectories on the transverse dispersion $\langle x_2^2 \rangle$ after 500 ms

Number of particle trajectories	10,000	20,000	40,000
$\langle x_2^2 \rangle$ (cm^2) Hollow glass			
Run 1	4.912	4.972	4.969
Run 2	4.973	4.996	4.983
$\langle x_2^2 \rangle$ (cm^2) Copper			
Run 1	1.693	1.714	1.711
Run 2	1.715	1.689	1.702

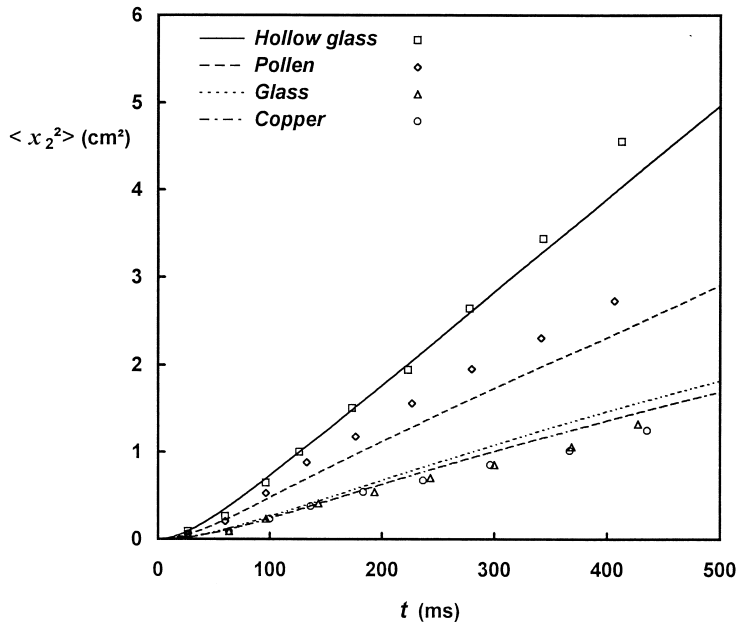

Fig. 2. Particle transverse dispersion in an upward uniform flow. Symbols: Experiments of Snyder and Lumley (1971). Lines: present predictions.

correlations. The advantage of the present method is that, even if the short time effects are not simulated as accurately as possible, the cumulative effects of all the previous time steps are correctly taken into account, thus preserving the representation of the coherent nature of the turbulence.

In order to examine the effect of gravity on particle dispersion, the mean square displacements of particles in the gravity direction have been studied. As can be seen in Fig. 3, which displays the dispersion ratio $\langle x_1^2\rangle/\langle x_2^2\rangle$, the streamwise particle dispersion is significantly larger than the transverse one, except for hollow glass particles. This means that particles

Table 3
Influence of the time step on the transverse dispersion $\langle x_2^2\rangle$ after 500 ms

	$\langle x_2^2\rangle$ (cm^2)	
	Run 1	Run 2
Hollow glass		
$\Delta t = 0.2$ ms	4.972	4.983
$\Delta t = 0.4$ ms	4.969	4.979
$\Delta t = 1.0$ ms	4.978	4.975
Copper		
$\Delta t = 0.5$ ms	1.702	1.713
$\Delta t = 1.0$ ms	1.714	1.689
$\Delta t = 2.0$ ms	1.692	1.714

disperse faster in the gravity direction, as predicted by previous studies (Reeks, 1977; Pismen and Nir, 1978). Such an anisotropy is due to the well-known continuity effect, a consequence of the drift velocity, which is here a function of the x_1-coordinate. As a result, this gravity induced anisotropy is increasing with increasing particle inertia, as shown by Fig. 3. It must be noticed that the particle dispersions in both transverse directions were found to be very close to one another, as could be expected since there is no preferential direction in the horizontal plane.

So far, the numerical code has been shown to yield satisfactory predictions of the behaviour of solid particles suspended in a turbulent uniform flow. In order to provide a first illustration of the effect of fluid shear on particle dispersion, calculations were also performed using the conditions of Huang and Stock's experiments, as described hereafter.

4.2. Simulation of the experiments of Huang and Stock (1997)

HS measured the particle dispersion in both transverse directions in a nearly homogeneous horizontal shear flow, created in a wind tunnel by means of a shear generator made up of parallel plates. The shear was in the vertical upwards direction, denoted here by x_2. The test section was about 0.36 m high and 2.4 m long. The mean velocity at the mid height of the test section was $\overline{V_{f_{1_0}}} = 5.925$ m/s, and the shear rate was $\chi = 10.69$ s^{-1}. The measured flow parameters were: $\sqrt{\overline{v_{f_1}^2}} \approx 0.23$ m/s, $\sqrt{\overline{v_{f_2}^2}} \approx 0.21$ m/s, $\sqrt{\overline{v_{f_3}^2}} \approx 0.23$ m/s, and $\overline{v_{f_1} v_{f_2}} \approx -0.021$ m^2/s^2. From these values, the one-point correlation coefficient used in the present simulation is $C_{12} \approx -0.4$. The turbulent kinetic energy dissipation rate ε can no longer be computed by

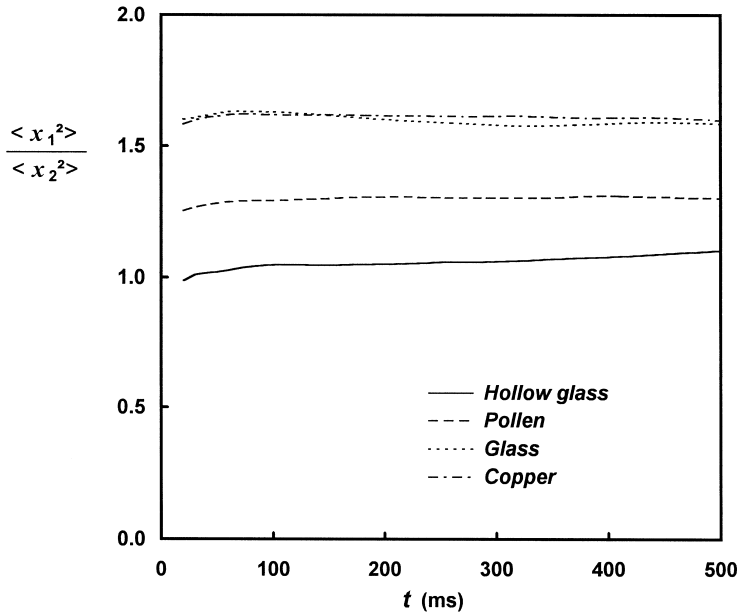

Fig. 3. Predicted streamwise-to-transverse dispersion ratio in the conditions of the experiments of Snyder and Lumley (1971).

Eq. (38), since we are concerned here with a non-decaying homogeneous turbulence. In this case, the turbulent kinetic energy equation leads to the following equilibrium condition between the dissipation and the turbulence production by the mean shear:

$$\varepsilon = -\overline{v_{f_1} v_{f_2}} \frac{d\overline{V_{f_1}}}{dx_2} = -\chi C_{12} \sqrt{\overline{v_{f_1}^2}} \sqrt{\overline{v_{f_2}^2}} \approx 0.23 \text{ m}^2/\text{s}^3 \tag{41}$$

Two types of glass beads, of density 2500 kg/m^3, diameter 24 and 51 μm, were injected in the centre of the section located at $x_1 = -0.0792$ m, and their dispersions $\langle x_2^2 \rangle$, $\langle x_3^2 \rangle$ were deduced from concentration profiles at three sections located between $x_1 = 1.55$ m and $x_1 = 2.11$ m.

The Lagrangian time scales of the fluid can be inferred from heat diffusion experiments performed by the authors, from which we can estimate $T_{22} \approx 70$ ms, and $T_{33} \approx 110$ ms. Assuming that such time scales obey the general expression similar to (37), namely:

$$T_{ii} = C_T \frac{\overline{v_{f_i}^2}}{\varepsilon} \tag{42}$$

we are led to the approximate value of the constant $C_T \approx 0.45$.

The length scales L_{ii} are still supposed to obey Eq. (39); however, contrary to the previous case, the coefficients C_{L2} and C_{L3} have to be different in order to account for the anisotropic nature of the flow. As shown by Champagne et al. (1970) who determined the spatial integral length scales in such a weak shear flow, L_{22} is about 1.6 times L_{33}, which means that we should have, according to the above mentioned values of the r.m.s. velocities, $C_{L2} \approx 2C_{L3}$.

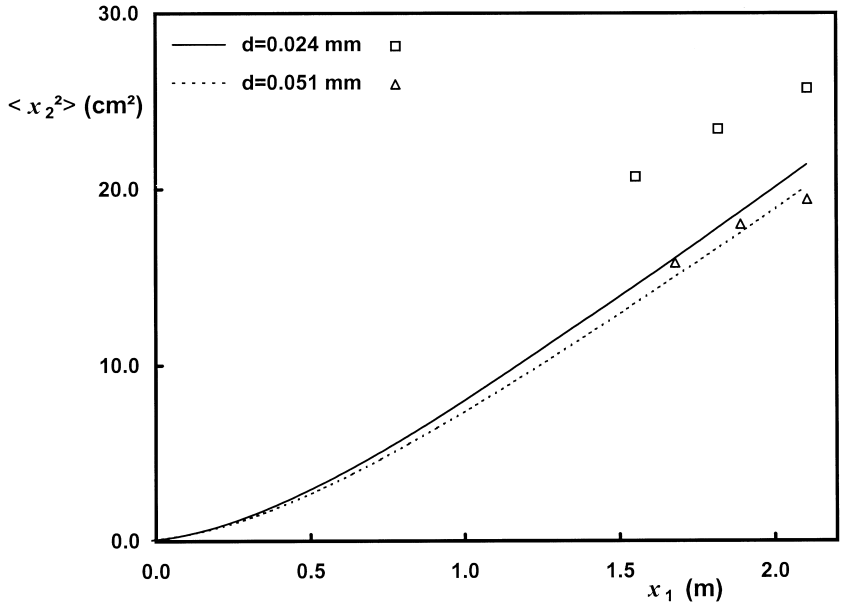

Fig. 4. Particle transverse dispersion (in the direction of shear) in a horizontal homogeneous shear flow. Symbols: Experiments of Huang and Stock (1997). Lines: present predictions.

Moreover, in accordance with the longitudinal Eulerian time scale measured by HS, which was about 15 ms, the spatial longitudinal time scale should be $L_{11} \approx 9$ cm, a value that can be obtained by choosing $C_{L1} \approx 4$. This is what we did in the simulations whose results are presented here, the final values of the constants being: $C_{L1} = C_{L2} = 4$, $C_{L3} = 2$.

Taking into account the particle relaxation time values, which are about 4 and 20 ms for the 24 and 51 μm particles, respectively, the time steps used for the simulation were $\Delta t = 0.5$ and 2 ms, respectively. From preliminary tests, no significant influence of Δt has been observed in performing calculations with four values of the time step, namely 0.2, 0.5, 1 and 2 ms, for each kind of particles.

Fig. 4 and Fig. 5 illustrate the comparison between our numerical predictions and the experimental data of HS, concerning the particle dispersion in direction x_2 and x_3, respectively. Except for the dispersion of the 24 μm particles in the direction of shear (direction x_2, Fig. 4), the numerical results can be seen to be in very good agreement with the experimental findings of HS. Taking the slope of the lines in Figs. 4 and 5, we obtain dispersion coefficients which are in qualitative agreement with the measurements of HS, even though the numerically predicted dispersion coefficient in case of the 51 μm particles in the direction perpendicular to the shear is significantly overestimated (Fig. 5). Concerning the observed discrepancy in Fig. 4 for the 24 μm particles, it should be mentioned that recent numerical results by Jiang et al. (1998), who simulated the same problem using the random Fourier modes method, are very similar to ours. In particular, the dispersion of the 24 μm particles in the direction of shear was also underestimated, even though the predicted dispersion coefficient, derived from the slope of the dispersion curves, is close to the experimental value. Moreover, in accordance with the

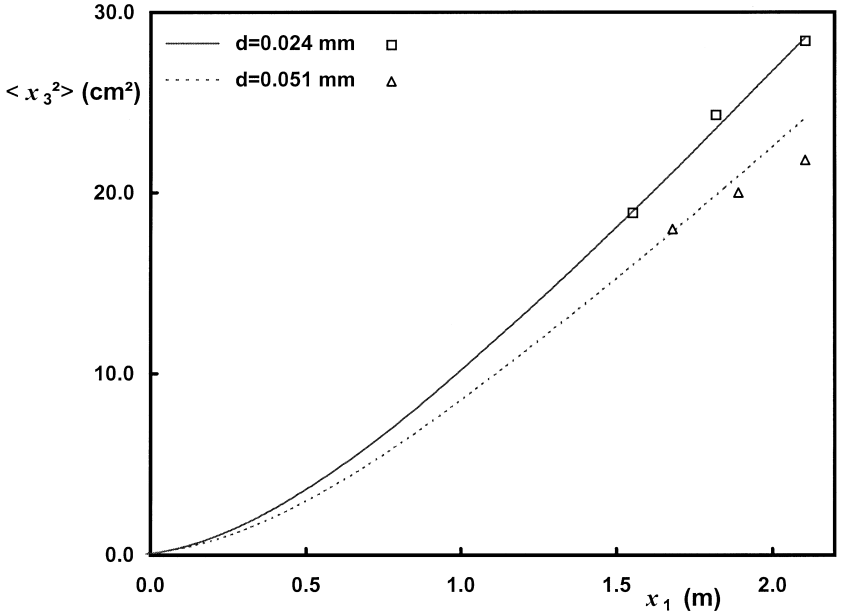

Fig. 5. Particle transverse dispersion (in the direction perpendicular to shear) in a horizontal homogeneous shear flow. Symbols: Experiments of Huang and Stock (1997). Lines: present predictions.

present predictions, it was also found by Jiang et al. (1998) that the dispersion difference between the 24 and 51 μm particles is larger in the x_3 direction. Actually, the reported values of $\langle x_2^2 \rangle$ by HS for the 24 μm particles seem to be surprisingly high, and it might therefore be asked whether some change in the upstream conditions could have caused any shift in the measurements.

The displayed numerical results have been obtained by including the lift force due to the mean fluid velocity gradient, as described in Section 2. Although it was found that the influence of lift does not exceed 3%, this transverse force was nevertheless taken into account for the investigation of particle dispersion in a vertical homogeneous shear flow, whose results are presented in the following section.

5. Particle dispersion predictions: results and discussion

In this section, the fluctuating motion of spherical particles suspended in an upward vertical turbulent air flow is investigated. The imposed mean velocity $\overline{V_{f_1}}$ obeys Eq. (2). The numerical investigation is carried out for the same four kinds of particles used by SL. Particles are supposed to be injected into the flow with an initial velocity equal to the local fluid velocity, so that the mean relative velocity is initially zero, and tends to the particle free fall velocity (or terminal velocity) for long dispersion time. Predictions concerning the effect of the mean fluid velocity gradient upon the particle dispersion and turbulent intensity are presented in Section 5.1. Results are further discussed in Section 5.2, with relevance to the analysis of Liljegren (1993).

5.1. Particle dispersion in a vertical homogeneous shear flow

Turbulent quantities of the vertical flow considered here are taken from the measurements obtained by Champagne et al. (1970) in a nearly homogeneous turbulent shear flow generated in a wind-tunnel. The centre-line mean velocity $\overline{V_{f_0}}$ was set at 12.4 m/s, and the mean shear rate was $\chi = 12.9\ \mathrm{s}^{-1}$. The intensity of the axial velocity fluctuation was perceptibly greater than of the other two components. The following values of turbulent intensities were measured in the working section:

$$\frac{\sqrt{\overline{v_{f_1}^2}}}{\overline{V_{f_{1_0}}}} = 0.018; \quad \frac{\sqrt{\overline{v_{f_2}^2}}}{\overline{V_{f_{1_0}}}} = 0.013; \quad \frac{\sqrt{\overline{v_{f_3}^2}}}{\overline{V_{f_{1_0}}}} = 0.014; \tag{43}$$

and the one-point correlation coefficient was

$$C_{12} = \frac{\overline{v_{f_1} v_{f_2}}}{\sqrt{\overline{v_{f_1}^2}}\sqrt{\overline{v_{f_2}^2}}} = -0.5 \tag{44}$$

In order to simulate the particle dispersion in such a shear flow, the Lagrangian time scales T_{ii} and the integral length scales L_{ii} are expressed by means of Eqs. (42) and (39), respectively, as was done for the second test case in the previous section, the dissipation ε being still computed

by Eq. (41). The coefficients C_T and C_{Li} were set at the same values, namely: $C_T = 0.45$, $C_{L1} = C_{L2} = 4$, $C_{L3} = 2$, which have been proven to yield satisfactory results in the horizontal shear flow of HS.

Calculations have been performed using the same particle densities and diameters as in Snyder and Lumley's experiments, under upward vertical air flow conditions. Particles are supposed to be injected at $x_1 = x_2 = 0$ with velocity $\overline{V_{f_0}}$. The effect of shear on particle dispersion is investigated by varying the mean shear rate from 4 to 20 s^{-1} (recalling that the actual shear rate in the experiments of Champagne et al. (1970) was 12.9 s^{-1}), and by examining the results about dispersions $\langle x_i x_j \rangle$, as well as particle velocity variances and dispersion coefficients D_{ij}, which are defined by

$$D_{ij}(t) = \frac{1}{2}\frac{d}{dt}\langle x_i x_j \rangle \tag{45}$$

and whose long-time values are estimated herein by

$$D_{ij\infty} \approx \frac{1}{2}\frac{\langle x_i x_j \rangle_{t_1} - \langle x_i x_j \rangle_{t_1 - \Delta t}}{\Delta t} \tag{46}$$

where $t_1 = 1500$ ms (see below) and $\Delta t = 20$ ms.

Owing to the proportionality between the turbulent kinetic energy dissipation rate and the velocity gradient, the resulting integral scales are inversely proportional to the shear rate. As a consequence, the particle Stokes number, defined here as $St = \tau_p / T_{11}$, is proportional to the velocity gradient χ, and this has to be taken into account in discussing the numerical predictions. Fig. 6 displays the Stokes number as a function of the shear rate for each kind of particles.

The duration t_1 of particle tracking was chosen in order to ensure that trajectories are computed during a sufficiently long time compared to the particle relaxation time and to the

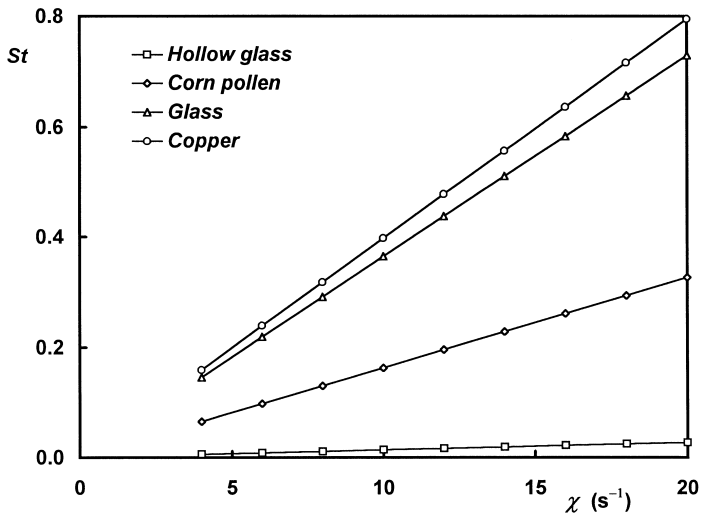

Fig. 6. Particle Stokes number as a function of the shear rate in the simulated vertical homogeneous shear flow.

turbulence integral time scale. Here, the largest particle relaxation time is about 50 ms, whereas the Lagrangian integral time scale T_{11} goes from 62 ms (for $\chi = 20\ s^{-1}$) to 310 ms (for $\chi = 4\ s^{-1}$). It was therefore decided to adopt $t_1 = 1500$ ms. The time step, which has to be sufficiently small compared to τ_p and T_{11}, was 0.2 ms for the hollow glass beads ($\tau_p = 1.7$ ms) and 2 ms for the other types of particles (whose relaxation time exceeds 20 ms). In each case, particle statistics was computed from 20,000 particle trajectories.

The general behaviour of the mean square displacements $\langle x_i^2 \rangle$ in such a shear flow is illustrated by Fig. 7, which displays an example of computed dispersions as a function of time for the lightest and the heaviest particles considered here. The main objective of this plot is to make clear the characteristic parabolic behaviour of the streamwise mean square displacement, due to both the growth of $\langle x_2^2 \rangle$ and the presence of the fluid velocity gradient, as pointed out by Liljegren (1993). There is therefore no constant asymptotic value of the dispersion coefficient in the streamwise direction, contrary to the transverse directions where the mean square displacements can be seen to vary linearly at sufficiently long time. The variance of the streamwise velocity, which is nonstationary, will be discussed in the next subsection with relevance to the theoretical work of Liljegren (1993). The influence of the shear rate on the streamwise mean square displacement at $t_1 = 1500$ ms is depicted by Fig. 8 for the four kinds of particles. Light particles are more affected by the shear than heavy particles. As could be expected due to the very close values of their relaxation time, glass and copper particles exhibit approximately the same dispersion characteristics whatever the mean fluid velocity gradient.

The particle dispersion in the transverse direction x_2 and the long-time dispersion coefficient D_{22} are illustrated by Fig. 9 and Fig. 10, respectively. The transverse particle dispersion can be seen to decrease with increasing shear rate, however, it must be recalled here that this is likely

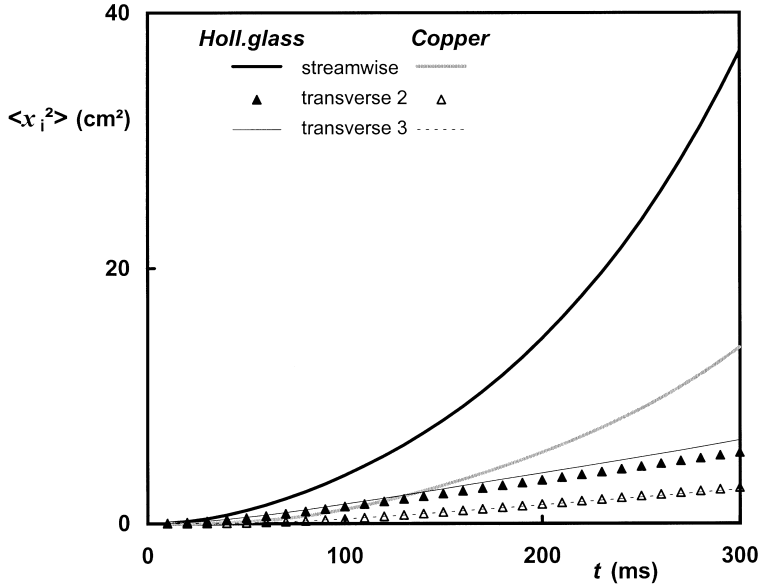

Fig. 7. Examples of the behaviour of the particle mean square displacements in the vertical homogeneous shear flow ($\chi = 14\ s^{-1}$).

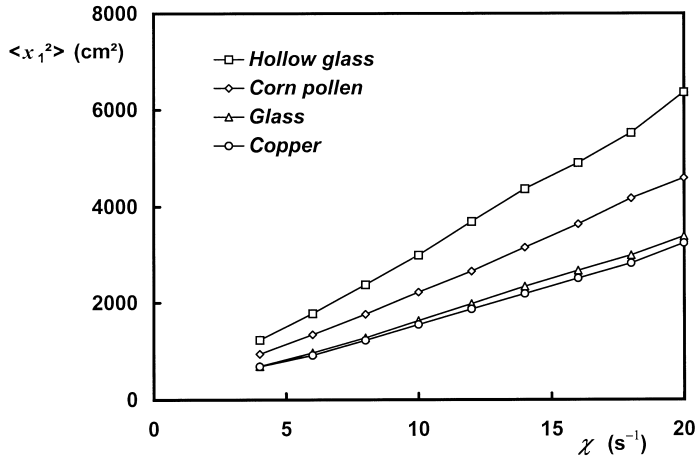

Fig. 8. Predicted streamwise dispersion, at $t_1 = 1500$ ms, as a function of the shear rate in the vertical homogeneous shear flow.

to be an effect of the Stokes number change according to Fig. 6, which means that the effect of particle inertia increases with increasing fluid shear rate. The direct influence of the velocity gradient can be made more explicit in examining the dispersion results at the same Stokes number: this can be done for the pollen, glass and copper particles in the range $St \approx 0.15$–0.35 (see Fig. 6). For example, for $St = 0.3$, which corresponds $\chi \approx 7.5$ for the copper beads and $\chi \approx 18$ for the corn pollen, the comparison shows that the presence of shear causes the pollen particles to disperse less than the copper particles, contrary to what would be expected in isotropic turbulence where crossing-trajectories effects are known to reduce the particle dispersion of heavier particles, due to their larger drift velocity (which is here the free fall velocity). It can be concluded that the effect of the fluid velocity gradient in such a vertical flow is to slightly reduce the transverse particle dispersion in the direction of shear. The ratio

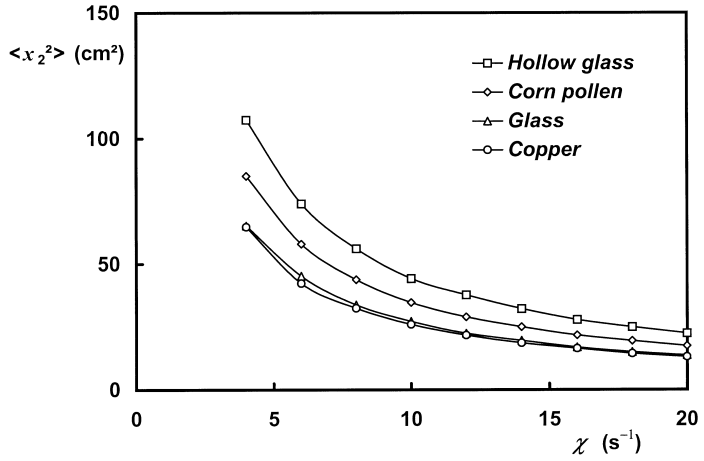

Fig. 9. Predicted transverse dispersion, at $t_1 = 1500$ ms, as a function of the shear rate.

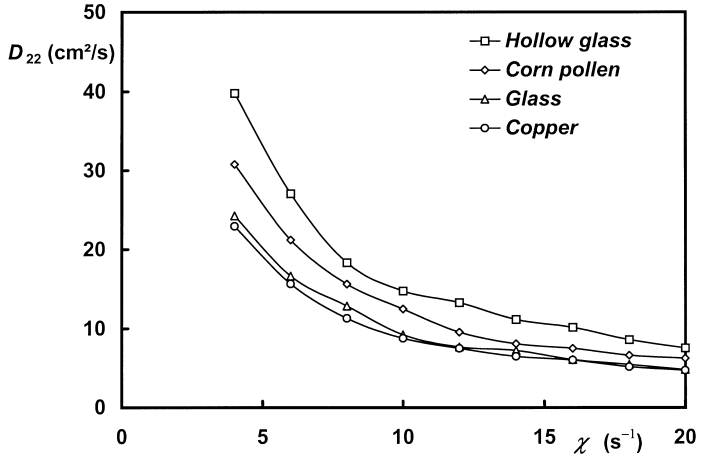

Fig. 10. Predicted long-time dispersion coefficient in the transverse direction, as a function of the shear rate.

of particle to fluid velocity variances in the same x_2-direction is plotted as a function of the shear rate in Fig. 11, which shows that the transverse velocity variance of light particles is not significantly modified by the presence of the velocity gradient, contrary to heavier particles. A comparison of particle velocity variances at a given value of the Stokes number shows that the direct influence of the shear on the particle transverse turbulent intensity is not significant, the observed decrease being mostly an effect of the Stokes number increase. Comparing the influence of the velocity gradient on the dispersion coefficient and on the particle turbulent intensity, it may be deduced that the effect of shear is to diminish the particle integral time scale in this transverse direction. The same conclusions may be drawn concerning the results in

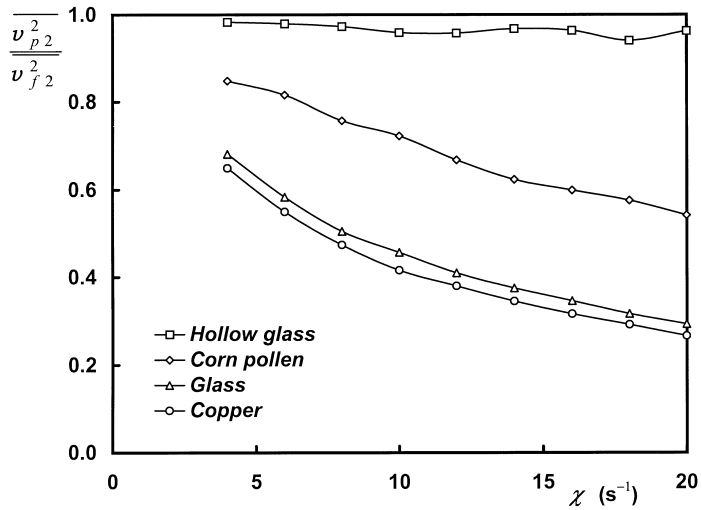

Fig. 11. Asymptotic value of the particle-to-fluid velocity variance ratio in the transverse direction.

the x_3-direction, where the only significant difference lies in the behaviour of the hollow glass particles, which are found to disperse faster than in the x_2-direction.

It is interesting to notice that a small mean transverse deviation $\langle x_{p_2} \rangle$ exists, except for the lightest particles, as illustrated by Fig. 12. Comparison between the predicted mean displacements $\langle x_{p_2} \rangle$ with and without taking the shear lift force into account shows that such an effect, which makes particles to deviate towards the larger velocity side, is largely reinforced by the lift force (which may be recalled to not significantly alter the dispersion properties presented herein, as already mentioned). However, the lateral deviation can be seen to exist for the heavier particles even without any effect of the lift force. Such a transverse deviation, which may possibly be due to non-linear drag effects, is not explained as yet, and will be subject to further investigations.

Results concerning the cross-dispersion are displayed by Fig. 13. Just after particle injection, and during a period of the order of the relaxation time, the displacement cross-correlation $\langle x_1 x_2 \rangle$ (calculated by $\langle x_1 x_2 \rangle = \langle x_{p_1} x_{p_2} \rangle - \langle x_{p_1} \rangle \langle x_{p_2} \rangle$) is negative, whatever the kind of particle (even if this cannot be seen in Fig. 13 for the hollow glass particles due to their very short relaxation time). The subsequent evolution towards large positive values is all the more rapid as the velocity gradient is higher. For long dispersion time, $\langle x_1 x_2 \rangle$ exhibits a parabolic behaviour similar to the streamwise dispersion $\langle x_1^2 \rangle$. This behaviour of the cross-dispersion $\langle x_1 x_2 \rangle$ is in accordance with the theory of turbulent diffusion of fluid particles in homogeneous shear flow, which predicts $\langle x_1 x_2 \rangle \approx \overline{v_{f_1} v_{f_2}} t^2$ for short diffusion times (leading to initially negative values of $\langle x_1 x_2 \rangle$) and $\langle x_1 x_2 \rangle \approx \chi \overline{v_{f_2}^2} T_{22} t^2$ for long diffusion times, where χ is the shear rate, leading to the observed parabolic behaviour (see Squires and Eaton, 1991). Since this behaviour physically results from the random nature of the particle position, which causes it to sample higher (if $x_2 > 0$) or lower (if $x_2 < 0$) mean fluid velocities, it could be expected that the solid particles behave in a qualitative similar manner.

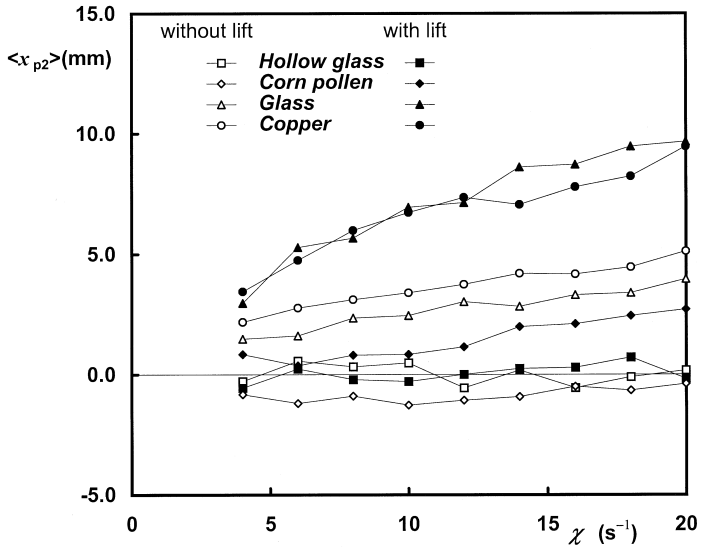

Fig. 12. Mean transverse deviation $\langle x_{p_2} \rangle$, at $t_1 = 1500$ ms, as a function of the shear rate.

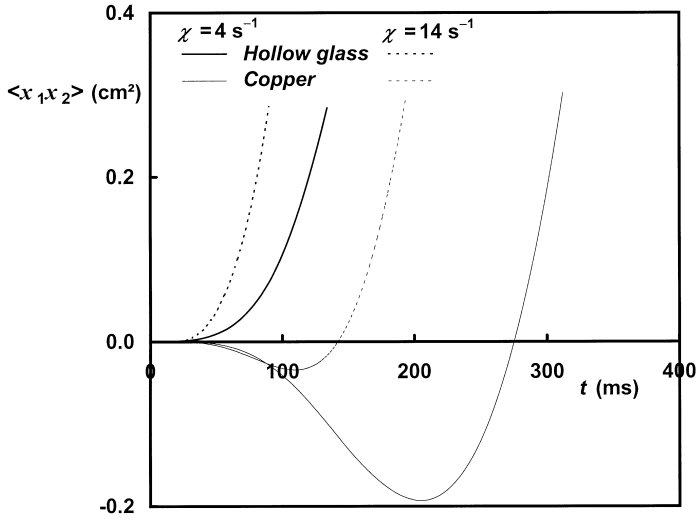

Fig. 13. Predicted displacement cross-correlation as a function of time in the initial stage of dispersion.

The progress in particle dispersion in a shear flow is depicted by Fig. 14 and Fig. 15, which illustrate the time evolution of the shape of the particle cloud for hollow glass beads and copper beads, respectively, with a shear rate $\chi = 14\ \mathrm{s}^{-1}$: the locations of 200 particles have been plotted at three successive values of the time t elapsed from injection. In both cases, the inclination of the particle cloud is changing from $t = 150$ ms, where $\langle x_1 x_2 \rangle \approx 0$ (or perceptibly less than zero for the copper particles), to $t = t_1 = 1500$ ms, where $\langle x_1 x_2 \rangle > 0$, according to the positive mean slope of the cloud (watch the x_1-axis scale change for $t = 1500$ ms). Moreover, the appearance of the mean transverse deviation, which is about 1 cm according to Fig. 12, can be discerned in case of heavy particles (Fig. 15), whereas Fig. 14 confirms that such a lateral deviation does not exist for very light particles.

5.2. Discussion

Liljegren (1993) investigated the effect of shear on the velocity variance of the particles, under the assumption of small particle Reynolds number (linear drag). In this case, the transverse velocity fluctuations of particles, which decrease with increasing Stokes number, were theoretically shown not to depend on the fluid velocity gradient. This is confirmed by the numerical results described above, recalling that the turbulent intensity decrease in Fig. 11 is due to the diminution of the fluid Lagrangian time scale with increasing shear, which makes the particle Stokes number to increase with the mean shear rate.

In order to compare the predictions about the streamwise particle motion with the theoretical analysis of Liljegren (1993), it is convenient to introduce the relative streamwise velocity between a particle and the mean fluid velocity at the current particle position:

$$W_{\mathrm{p}_1} = V_{\mathrm{p}_1} - \left(\overline{V_{\mathrm{f}_{1_0}}} + \chi x_{\mathrm{p}_2} \right) \tag{47}$$

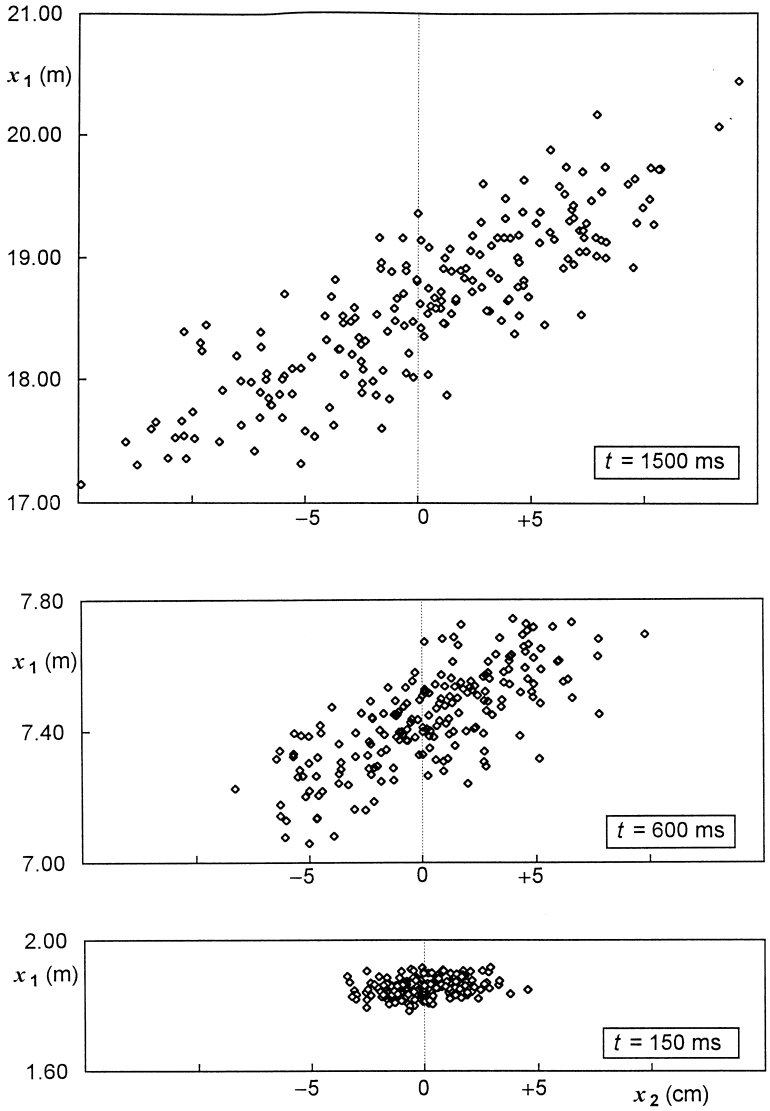

Fig. 14. Particle clouds at $t = 150$, 600 and 1500 ms (hollow glass particles, $\chi = 14\ s^{-1}$).

which is stationary in variance (denoted hereafter by $\overline{w_{p_1}^2}$) as are the transverse components of the particle velocity. At the low Stokes number limit, Liljegren (1993) showed that the particle relative velocity variance obeys the following relationship:

$$\frac{\overline{w_{p_1}^2}}{\overline{v_{f_1}^2}} - \frac{\overline{v_{p_2}^2}}{\overline{v_{f_2}^2}} = 2\chi\tau_p \frac{|\overline{v_{f_1} v_{f_2}}|}{\overline{v_{f_1}^2}} \tag{48}$$

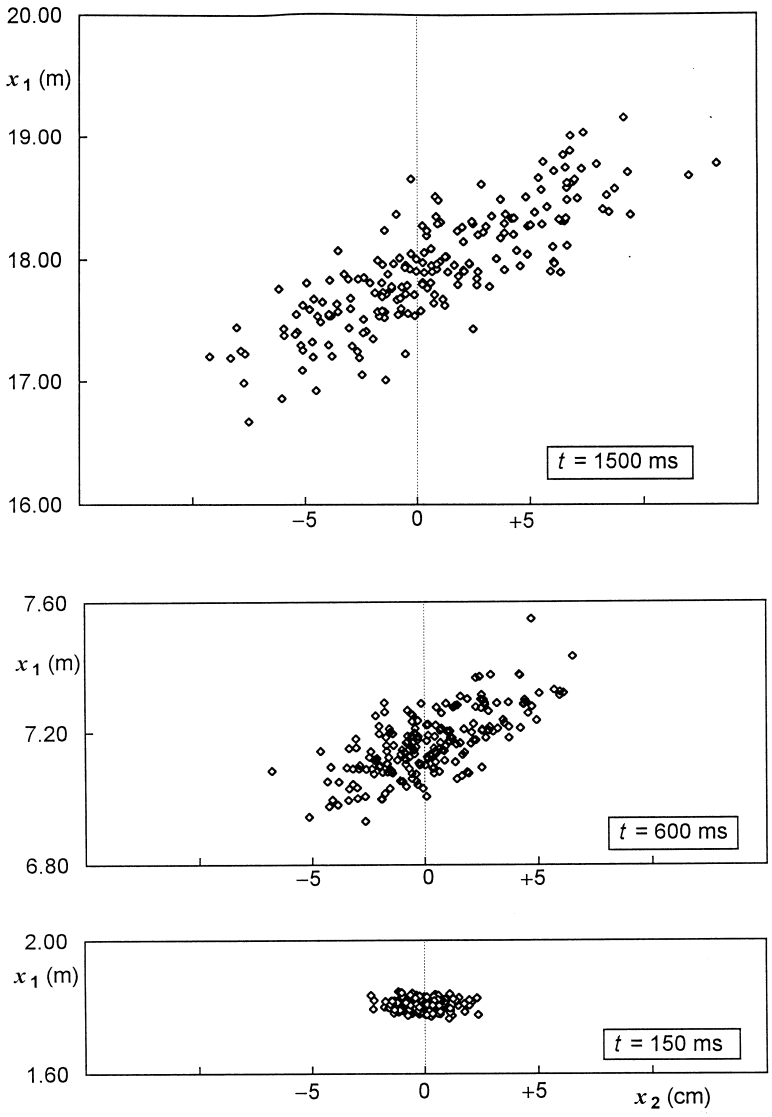

Fig. 15. Particle clouds at $t = 150$, 600 and 1500 ms (copper particles, $\chi = 14\ s^{-1}$).

which is displayed by the lines in Fig. 16, and compared to our numerical predictions. A good agreement is obtained for the hollow glass particles, which satisfy the condition of small Stokes number. For the heavier particles (whose Reynolds number exceeds unity) the computed values are still in qualitative agreement with the theoretical ones, however it can be seen that the difference $(\overline{w_{p_1}^2}/\overline{v_{f_1}^2}) - (\overline{v_{p_2}^2}/\overline{v_{f_2}^2})$ tends to a constant value for the glass and copper particles as soon as the velocity gradient exceeds about 10, a range corresponding to Stokes number which are beyond the validity limit of Liljegren's analysis.

The observed phenomena are therefore in accordance with the conclusions of the theoretical

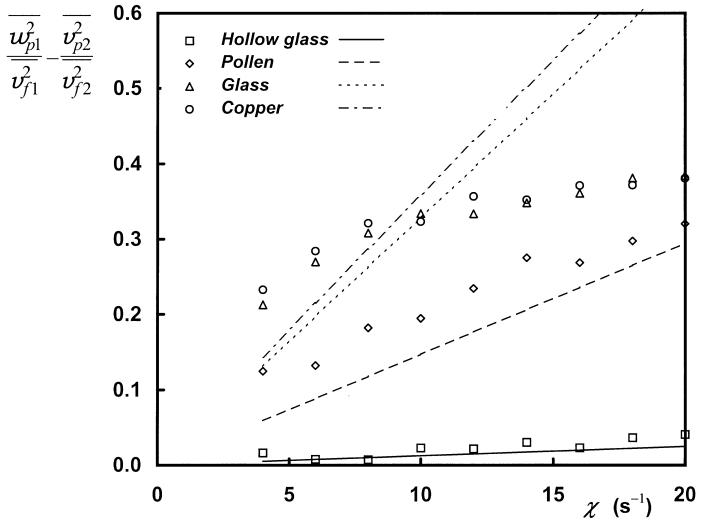

Fig. 16. Comparison between the numerical predictions and the theoretical result of Liljegren (1993) concerning the variance of the streamwise relative velocity.

analysis of Liljegren (1993) for low particle Stokes numbers. As shown by Fig. 13, the effect of the fluid Reynolds stress is prevailing at short dispersion time (compared to τ_p) and low shear rate, leading to negative values of $\langle x_1 x_2 \rangle$. After this initial period, the cross-dispersion is positive, meaning that, on average, the x_1-coordinate of a particle located at $x_2 > 0$ exceeds the mean value $\overline{x_1}$, and inversely for a particle at location $x_2 < 0$. This can be explained by considering the changes in the fluid velocity encountered by particles during their fluctuating motion. In the presence of shear, and owing to their transverse random walk, particles undergo fluid velocity differences which are not only due to the fluid turbulent fluctuations but also to the variations in the mean fluid velocity, which is depending on the instantaneous location of the particle along the x_2-direction. Therefore, particles tend to have a larger streamwise displacement, i.e., dispersion, relative to particles moving in a uniform turbulent flow. As pointed out by Liljegren (1993), such a mechanism can explain some experimental results reported in the literature. Among others, Tsuji and Morikawa (1982) measured such large streamwise particle velocity fluctuations in a pipe flow, and Rogers and Eaton (1990) reported similar results in a boundary layer.

6. Conclusion

In order to analyse the effects of a mean fluid velocity gradient on the behaviour of suspended particles in a turbulent gas flow, an anisotropic Lagrangian tracking technique, based on the approach proposed by Burry and Bergeles (1993), was used. Emphasis was put on the choice of consistent correlation matrices with respect to the first-order time-series used to determine the fluid velocity fluctuations. Numerically predicted transverse particle dispersions have been satisfactorily confronted to Snyder and Lumley's experimental results in case of

uniform flow, as well as to Huang and Stock's measurements in a horizontal homogeneous shear flow. Finally, the numerical simulation was used for the prediction of particle dispersion in a vertical upward turbulent air flow, in taking the influence of gravity into account.

Original results have been obtained about the fluctuating and mean motion of particles in the presence of a uniform mean velocity gradient. The variance of the streamwise particle relative velocity has been found to increase above the level predicted without shear, in accordance with the theoretical analysis of Liljegren (1993). Except at low shear rate or short dispersion time, the main mechanism by which the streamwise dispersion is increased is through the random interaction of the particles with the mean fluid velocity gradient, as has been shown by examining the cross-dispersion results. The transverse particle dispersion has been found to be unaffected by the shear, as predicted by Liljegren (1993), in case of small particle Reynolds number. Although Liljegren's analysis was restricted to the flows where the particle Reynolds number is low enough for the drag force to obey the Stokes' law, the above predictions show that her qualitative conclusions are confirmed in case of non-linear drag.

The influence of the lift force induced by the mean shear upon the particle dispersion has been found to be negligible, except for the mean transverse deviation which has been observed for heavier particles. However, such a lateral deviation of the particle cloud has been proved not to be caused only by the lift force. Explanation of such a phenomena will require additional investigations.

Further developments will include the improvement of the techniques based on the simultaneous tracking of a solid particle and a fluid tracer, by adapting the method to more elaborate stochastic processes, thus making it possible to use more realistic correlation matrices. From the present results, which confirm and extend Liljegren's qualitative analysis, and which provide new information about the particle behaviour in a turbulent shear flow, it can be concluded that such phenomena should be taken into account in analyses of particulate two-phase flows.

Appendix A. Drag and lift coefficient correlations

A.1. Correlation of Morsi and Alexander (1972)

$$C_D = k_1 + \frac{k_2}{Re_p} + \frac{k_3}{Re_p^2} \tag{A1}$$

The coefficients k_1, k_2, k_3, are listed in Table 4.

A.2. Correlation of Mei (1992)

$Re_p \leq 40$:

Table 4
Coefficients k_1, k_2 and k_3

	k_1	k_2	k_3
$Re_p \leq 0.1$	0	24	0
$0.1 < Re_p \leq 1$	3.69	22.73	0.0903
$1 < Re_p \leq 10$	1.222	29.167	−3.889
$10 < Re_p \leq 10^2$	0.6167	46.5	−116.67
$102 < Re_p \leq 10^3$	0.3644	98.33	−2778

$$C_L = 4.113\frac{Re_\chi^{1/2}}{Re_p}\left[\left(1 - 0.3314\left(\frac{Re_\chi}{2Re_p}\right)^{1/2}\right)\exp\left(-\frac{Re_p}{10}\right) + 0.3314\left(\frac{Re_\chi}{2Re_p}\right)^{1/2}\right] \quad \text{(A2)}$$

$40 < Re_p \leq 100$:

$$C_L = 0.1524\frac{Re_\chi}{Re_p} \quad \text{(A3)}$$

References

Berlemont, A., Desjonqueres, P., Gouesbet, G., 1990. Particle Lagrangian simulation in turbulent flows. Int. J. Multiphase Flow 16, 19–34.

Burnage, H., Moon, S., 1990. Prédétermination de la dispersion de particules matérielles dans un écoulement turbulent. C. R. Acad. Sci. Paris II-310, 1595–1600.

Burry, D., Bergeles, G., 1993. Dispersion of particles in anisotropic turbulent flows. Int. J. Multiphase Flow 19, 651–664.

Champagne, F.H., Harris, V.G., Corrsin, S., 1970. Experiments on nearly homogeneous turbulent shear flow. J. Fluid Mech 41, 81–139.

Chen, P.P., Crowe, C.T., 1984. On the Monte–Carlo modelling particle dispersion in turbulence. In: Proc. Int. Symp. on Gas–Solid Flows. ASME FED vol. 10, 37–41.

Chen, X.Q., Pereira, J.C.F., 1997. Efficient computation of particle dispersion in turbulent flows with a stochastic-probabilistic model. Int. J. Heat Mass Transfer 40, 1727–1741.

Corssin, S., Lumley, J., 1956. On the equation of motion for a particle in turbulent fluid. Appl. Sci. Res A. 6, 114–116.

Crowe, C.T., Troutt, T.R., Chung, J.N., 1996. Numerical models for two-phase turbulent flows. Annu. Rev. Fluid. Mech 28, 11–43.

Dandy, D.S., Dwyer, H.A., 1990. A sphere in shear flow at finite Reynolds number: effect of shear on particle lift, drag and heat transfer. J. Fluid Mech 216, 381–410.

Gatignol, R., 1983. The Faxen formulae for a rigid particle in an unsteady non-uniform Stokes flow. J. Mécanique Théorique et Appliquée 2, 143–160.

Gosman, A.D., Ioannides, E., 1981. Aspects of computer simulation of liquid-fuelled combustors. In: Proc. of the AIAA 19th Aerospace Science Meeting, St. Louis, MO paper 81-0323.

Gouesbet, G., Berlemont, A., Picart, A., 1982. On the Tchen's theory of discrete particle dispersion: can dense discrete particles disperse faster than fluid? . Letters in Heat and Mass Transfer 9, 407–419.

Gouesbet, G., Berlemont, A., Picart, A., 1984. Dispersion of discrete particles by continuous turbulent motions.

Extensive discussion of the Tchen's theory, using a two-parameter family of Lagrangian correlation functions. Phys. Fluids 27, 827–836.
Graham, D.I., 1998. Analytical comparison of Lagrangian particle dispersion models, In: Proc. ICMF'98, 3rd Int. Conf. Multiphase Flow, Lyon, France, paper 125.
Harvey, A.C., 1989. Forecasting, structural time series models and the Kalman filter. Cambridge University Press, Cambridge, UK.
Hetsroni, G., 1989. Particles-turbulence interaction. Int. J. Multiphase Flow 15, 735–746.
Hinze, J.O., 1975. Turbulence, 2nd ed. McGraw-Hill, New-York.
Huang, X., Stock, D.E., 1997. Measurements of particle dispersion in a uniform shear flow. In: Proc. ASME FED, Vancouver, Canada paper FEDSM97-3627.
Huilier, D., Saintlos, S., Karl, J.J., Burnage, H., 1996. Numerical modelling of the turbulent dispersion of heavy particles: inertia and gravity effects on turbulent diffusivity. In: Rodi, W., Bergeles, G. (Eds.), Proc. 3rd Int. Symp. on Engineering Turbulence Modelling and Measurements, Heraklion-Crete, Greece. Elsevier, Amsterdam, pp. 861–870.
Jiang, Y., Huang, X., Stock, D.E., 1988. Using random Fourier modes to simulate particle dispersion in a uniform shear flow. In: Proc. ICMF'98, 3rd Int. Conf. Multiphase Flow, Lyon, France paper 634.
Liljegren, L.M., 1993. The effect of a mean fluid velocity gradient on the streamwise velocity variance of a particle suspended in a turbulent flow. Int. J. Multiphase Flow 19, 471–484.
Lu, Q.Q., Fontaine, J.R., Aubertin, G., 1993. A Lagrangian model for solid particles in turbulent flows. Int. J. Multiphase Flow 19, 347–367.
MacLaughlin, J.B., 1991. Inertial migration of a small sphere in linear shear flows. J. Fluid Mech 224, 261–274.
Maxey, M.R., Riley, J.J., 1983. Equation of motion for a small rigid sphere in a non uniform flow. Phys. Fluids 26, 883–889.
Mei, R., 1992. An approximate expression for the shear lift force on a spherical particle at finite Reynolds number. Int. J. Multiphase Flow 18, 145–147.
Mei, R., Adrian, R.J., 1992. Flow past a sphere with an oscillation in the free-stream velocity and unsteady drag at finite Reynolds number. J. Fluid Mech 237, 323–441.
Morsi, S.A., Alexander, A.J., 1972. An investigation of particle trajectories in two-phase flow systems. J. Fluid Mech 55, 193–208.
Odar, F., 1966. Verification of the proposed equation for calculation of the forces on a sphere accelerating in a viscous fluid. J. Fluid Mech 25, 591–592.
Ormancey, A., Martinon, J., 1984. Prediction of particle dispersion in turbulent flows. Phys. Chem. Hydrodynamics 5, 229–244.
Peskin, R.L., Kau, C.J., 1976. Numerical simulation of particulate motion in turbulent gas–solid channel flow. ASME-Paper, 76-WA/FE-37.
Pismen, L.M., Nir, A., 1978. On the motion of suspended particles in stationary homogeneous turbulence. J. Fluid Mech 84, 193–206.
Reeks, M.W., 1977. On the dispersion of small particles suspended in an isotropic turbulent fluid. J. Fluid Mech 83, 529–546.
Rogers, C.B., Eaton, J.K., 1990. The behavior of solid particles in a vertical turbulent boundary layer in air. Int. J. Multiphase Flow 16, 819–834.
Saffman, P.G., 1965. The lift on a small sphere in a slow shear flow. J. Fluid Mech 22, 385–400.
Saffman, P.G., 1968. Corrigendum. J. Fluid Mech 31, 624.
Sawford, B.L., 1991. Reynolds number effects in Lagrangian stochastic models of turbulent dispersion. Phys. Fluids A 3, 1577–1586.
Shirolkar, J.S., Coimbra, C.F.M., McQuay, M.Q., 1996. Fundamental aspects of modeling turbulent particle dispersion in dilute flows. Prog. Energy Combust. Sci 22, 363–399.
Shirolkar, J.S., McQuay, M.Q., 1998. Probability density function propagation model for turbulent particle dispersion. Int. J. Multiphase Flow 24, 663–678.
Snyder, W.H., Lumley, J.L., 1971. Some measurements of particle velocity autocorrelation functions in a turbulent flow. J. Fluid Mech 48, 41–71.

Soo, S.L., Ihrig, H.K., El Kouh, A.F., 1960. Experimental determination of statistical properties of two-phase turbulent motion. J. Basic Engng., Trans. ASME 82, 609–621.

Squires, K.D., Eaton, J.K., 1991. Lagrangian and Eulerian statistics obtained from direct numerical simulations of homogeneous turbulence. Phys. Fluids A 3, 130–143.

Tchen, C.M., 1947. Mean value and correlation problems connected with the motion of small particles suspended in a turbulent fluid. Ph.D. Thesis, University of Delft, Martinus Nijhoff, The Hague.

Tsuji, Y., Morikawa, Y., 1982. LDV measurements of an air–solid two-phase flow in a horizontal pipe. J. Fluid Mech 120, 385–409.

Ushijima, T., Perkins, R., 1998. Two-point velocity correlation of separating fluid element and heavy particle. In: Proc. ICMF'98, 3rd Int. Conf. Multiphase Flow, Lyon, France, paper 701.

Wang, L.P., Stock, D.E., 1993. Dispersion of heavy particles by turbulent motion. J. Atmosph. Sci 50, 1897–1913.

Yarin, L.P., Hetsroni, G., 1994a. Turbulence intensity in dilute two-phase flows—1. Effect of particle-size distribution on the turbulence of the carrier fluid. Int. J. Multiphase Flow 20, 1–15.

Yarin, L.P., Hetsroni, G., 1994b. Turbulence intensity in dilute two-phase flows—3. The particles-turbulence interaction in dilute two-phase flow. Int. J. Multiphase Flow 20, 27–44.

Zhou, Q., Leschziner, M.A., 1991. A time-correlated stochastic model for particle dispersion in anisotropic turbulence. In: Proc. 8th Symp. on Turbulent Shear Flows, Munich, Germany, 10.3.1–10.3.6.

Zhou, Q., Leschziner, M.A., 1996. Modelling particle dispersion in anisotropic turbulence. In: Proc. ECCOMAS Comput. Fluid Dynamics Conf., Paris, France, 577–583.